Preprint typeset using LaTeX style emulateapj v. 08/22/09

arXiv:0805.4416v1 [astro-ph] 29 May 2008

THE DARK MATTER ANNIHILATION SIGNAL FROM GALACTIC SUBSTRUCTURE: PREDICTIONS FOR GLAST

Michael Kuhlen[1], Jürg Diemand[2,3], Piero Madau[2]
[1]School of Natural Sciences, Institute for Advanced Study, Einstein Lane, Princeton, NJ 08540
[2]Department of Astronomy & Astrophysics, University of California, Santa Cruz, CA 95064
[3]Hubble Fellow

ABSTRACT

We present quantitative predictions for the detectability of individual Galactic dark matter subhalos in gamma-rays from dark matter pair annihilations in their centers. Our method is based on a hybrid approach, employing the highest resolution numerical simulations available (including the recently completed one billion particle Via Lactea II simulation) as well as analytical models for the extrapolation beyond the simulations' resolution limit. We include a self-consistent treatment of subhalo boost factors, motivated by our numerical results, and a realistic treatment of the expected backgrounds that individual subhalos must outshine. We show that for reasonable values of the dark matter particle physics parameters ($M_\chi \sim 50 - 500$ GeV and $\langle\sigma v\rangle \sim 10^{-26} - 10^{-25}$ cm^3 s^{-1}) GLAST may very well discover a few, even up to several dozen, such subhalos, at 5 σ significance, and some at more than 20 σ. We predict that the majority of luminous sources would be resolved with GLAST's expected angular resolution. For most observer locations the angular distribution of detectable subhalos is consistent with a uniform distribution across the sky. The brightest subhalos tend to be massive (median $V_{\rm max}$ of 24 km s^{-1}) and therefore likely hosts of dwarf galaxies, but many subhalos with $V_{\rm max}$ as low as 5 km s^{-1} are also visible. Typically detectable subhalos are $20 - 40$ kpc from the observer, and only a small fraction are closer than 10 kpc. The total number of observable subhalos has not yet converged in our simulations, and we estimate that we may be missing up to 3/4 of all detectable subhalos.

Subject headings: dark matter – Galaxy: structure – galaxies: halos – gamma rays: theory – methods: n-body simulations

1. INTRODUCTION

Revealing the nature of dark matter is fundamental to cosmology and particle physics. In the standard cosmological paradigm of structure formation (ΛCDM), the universe is dominated by cold, collisionless dark matter (CDM), and endowed with initial density perturbations via quantum fluctuations during inflation. In this model galaxies form hierarchically, with low-mass objects ("halos") collapsing earlier and merging to form larger and larger systems over time. Small halos collapse at high redshift when the universe is very dense, so their central densities are correspondingly high. When these halos merge into larger hosts, their high densities allow them to resist the strong tidal forces that act to destroy them. It is therefore a clear, unique prediction of ΛCDM that galaxies are embedded in massive, extended dark matter halos teeming with self-bound substructure or "subhalos".

If the dark matter is in the form of a relic particle once in thermal equilibrium in the early universe, like the neutralino in SUSY, then substructures will be lit up by pair annihilations of these particles into standard model particles, whose subsequent decay results in gamma-ray emissions. The signal depends on unknown conjectured particle physics properties and poorly known astrophysical parameters. Particle physics uncertainties include the type of particle (axion, neutralino, Kaluza-Klein particle, etc.), its mass, and its pair annihilation cross-section. From the astrophysical side, since the annihilation rate is proportional to density squared, the predicted flux depends sensitively on the clumpiness of the mass distribution.

The detection of annihilation radiation from DM clumps is surely one of the most exciting discoveries that the upcoming *Gamma-ray Large Area Space Telescope* (GLAST) could make. Currently scheduled to be launched in May of 2008, GLAST is NASA's successor to the Compton Gamma Ray Observatory, whose EGRET instrument conducted the first all-sky gamma-ray survey and discovered 271 sources, 170 of which remain unidentified (Hartman et al. 1999). GLAST will carry two instruments, the GLAST Burst Monitor (GBM), designed to detect flashes from gamma-ray bursts and solar flares, and the Large Area Telescope (LAT), the main survey instrument. The LAT consists of several layers of high-precision silicon tracking detectors for determining the direction of an incident gamma-ray, a cesium-iodide calorimeter to measure its total energy, and an anticoincidence detector for cosmic ray rejection.

With a field of view of about 2.4 sr and a 90 minute orbital period, the LAT will survey the entire sky daily. Its peak effective area exceeds 8000 cm^2 beyond 1GeV and its angular resolution ranges from $< 3.5^\circ$ at 100 MeV down to < 9 arcmin above 10 GeV. Compared to EGRET, the LAT has a 4-5 times larger field of view, more than 5 times larger peak effective area, 5-40 times higher angular resolution above 1 GeV, and ~ 30 times better point source sensitivity. Additionally, the LAT detector is sensitive to gamma-rays out to 300 GeV, ten times higher than EGRET's limit. Given these improvements it is not unreasonable to hope that GLAST will discover previously unknown sources, one of which may

TABLE 1
Simulation Parameters

Name	$L_{\rm box}$ (Mpc)	ϵ (pc)	z_i	$N_{\rm hires}$	$M_{\rm hires}$ ($M_\odot$)	r_{200} (kpc)	M_{200} ($M_\odot$)	$V_{\rm max}$ (km s^{-1})	$r_{\rm Vmax}$ (kpc)	$N_{\rm sub}$
VL-I	90.0	90.0	48.4	2.34×10^8	2.1×10^4	389	1.77×10^{12}	181	69	9,224
VL-II	40.0	40.0	104.3	1.09×10^9	4.1×10^3	402	1.93×10^{12}	201	60	53,653

Note. — Box size $L_{\rm box}$, (spline) softening length ϵ, initial redshift z_i, number $N_{\rm hires}$ and mass $M_{\rm hires}$ of high resolution dark matter particles, host halo r_{200}, M_{200}, and $V_{\rm max}$, and number of subhalos within r_{200} $N_{\rm sub}$ for the VL-I and VL-II simulations. Force softening lengths ϵ are constant in physical units back to $z = 9$ and constant in comoving units before.

be annihilating DM in the centers of Galactic subhalos.

What region in the sky is mostly likely to allow for a detection of gamma-rays from DM annihilations is a hotly contested question. The Galactic center (GC) is likely the largest nearby DM overdensity and a number of studies have advocated it as the best place to look for a signal (Berezinsky et al. 1994; Bergström et al. 1998, 2001; Ullio et al. 2002; Cesarini et al. 2004). A major drawback for this scenario, however, is the large astrophysical gamma-ray background near the GC. Furthermore, the lack of a spectral break below ~ 30 TeV in the recent H.E.S.S. (Aharonian et al. 2006) and MAGIC (Albert et al. 2006) measurements of the very high energy gamma-ray emission from the GC severely limits the contribution that annihilating DM particles with masses less than $\mathcal{O}(10$ TeV) can make to this signal. Instead, Stoehr et al. (2003) suggested to focus observations on an annulus between 25° and 35° from the Galactic center, since this would maximize the chances of detection by reducing the background while simultaneously avoiding numerical uncertainties in the central DM density profile. Perhaps more promising is the possibility of detecting DM annihilation from the centers of Galactic subhalos, either from one of the known Milky Way dwarf satellite galaxies or from a nearby dark clump (Bergström et al. 1999; Baltz et al. 2000; Calcáneo-Roldán & Moore 2000; Tasitsiomi & Olinto 2002; Stoehr et al. 2003; Taylor & Silk 2003; Evans et al. 2004; Aloisio et al. 2004; Koushiappas et al. 2004; Koushiappas 2006; Diemand et al. 2007a; Strigari et al. 2007b; Pieri et al. 2008). Lastly, an additional source population might arise from local DM density enhancements (mini-spikes) around black hole remnants of the first generation of stars (Bertone et al. 2005b).

If GLAST detects photons originating in pair annihilations of DM particles in the centers of subhalos, will it be possible to distinguish this signal from conventional astrophysical gamma-ray sources? While a definite answer to this question will have to await actual GLAST data, Baltz et al. (2007) have argued that this should be possible based on four criteria: (i) a hadronic spectrum from monochromatic quarks, (ii) lack of time variability, (iii) spatial extent, and (iv) a lack of emission at shorter wavelengths, except for very diffuse inverse Compton and synchrotron radiation (Baltz & Wai 2004; Colafrancesco et al. 2006, 2007). Gamma-ray pulsars are probably the most problematic astrophysical sources in this regard, owing to the similarity of their spectra to a typical DM annihilation spectrum. Fortunately they tend to lie in the Galactic plane, often exhibit X-ray counterparts, and are point-like.

The observability of DM annihilation radiation originating in Galactic subhalos depends on their abundance, distribution, and internal structure, properties which must be determined by numerical simulation, since they are the result of structure formation in the highly non-linear regime. Previous investigations have typically only indirectly made use of numerical simulations, employing (semi-)analytic models that have been calibrated to published numerical results. Often these results were derived from simulations that do not resolve the relevant sub-galactic scales, and it is not clear that a simple extrapolation is justified, since not all substructure properties are scale invariant. Some past work (Calcáneo-Roldán & Moore 2000; Stoehr et al. 2003; Diemand et al. 2006; Athanassoula et al. 2008) has directly used numerical simulations, but these studies either suffered from insufficient resolution, didn't correct for effects from the population of unresolved subhalos, or didn't realistically account for the gamma-ray backgrounds against which individual subhalos must compete.

Ground based gamma-ray detectors, i.e. atmospheric Cerenkov telescopes (ACT) like H.E.S.S., VERITAS, MAGIC, and STACEE will provide complementary information to GLAST's observations. However, owing to the comparatively small field of view of ACT's, the detection of individual subhalos with such observations would either have to rely on serendipity to provide a detectable subhalo in the surveyed portion of the sky, or they would have to target a known likely source such as a nearby dark matter dominated dwarf galaxy (e.g. Albert et al. 2008; Sánchez-Conde et al. 2007; Driscoll et al. 2007). As advocated by Koushiappas et al. (2004), a better strategy might be to locate sources with GLAST and then conduct follow-up observations with an ACT to measure the gamma-ray spectrum out to higher energies.

Motivated by the imminent launch of the GLAST satellite, we present here a comprehensive analysis of the detectability of individual DM subhalos, taylored to GLAST expectations. Our method is based on a hybrid approach, combining the highest resolution numerical simulations of the distribution of Galactic DM substructure (described in § 2.1) with analytical models for the extrapolation of the substructure hierarchy below the simulations' resolution limit. We include a self-consistent treatment of subhalo boost factors (§ 2.2), motivated by our numerical results, and a realistic treatment of the expected backgrounds that individual subhalos must outshine (§ 3.1). We consider a physically motivated region of particle physics parameter space (§ 3.2) and check that our results don't violate existing EGRET constraints (§ 3.3). Our analysis results in quantitative predictions for the number of observable subhalos as a function of particle physics parameters (§ 3.4), and we also consider the possibility of detecting microhalos be-

low $1\,M_\odot$ (§ 3.5). A discussion of our results and conclusions can be found in § 4.

2. MODELS AND METHODOLOGY

The number of DM annihilation gamma-ray photons from a solid angle $\Delta\Omega$ along a given line of sight (θ, ϕ) over an integration time of $\tau_{\rm exp}$ is given by

$$N_\gamma(\theta,\phi) = \frac{\Delta\Omega}{4\pi}\,\tau_{\rm exp}\frac{\langle\sigma v\rangle}{2M_\chi^2}\left[\int_{E_{\rm th}}^{M_\chi}\left(\frac{dN_\gamma}{dE}\right)A_{\rm eff}(E)dE\right] \times\int_{\rm los}\rho(l)^2 dl. \quad (1)$$

This expression contains terms that depend a) on the properties of the detector (the angular resolution $\Delta\Omega$, the energy dependent effective area $A_{\rm eff}(E)$, the energy threshold $E_{\rm th}$, and the total exposure time $\tau_{\rm exp}$), b) on the chosen particle physics model describing the nature of the DM particle (i.e. its mass M_χ and thermally averaged velocity-weighted annihilation cross section $\langle\sigma v\rangle$, and the photon spectrum due to a single annihilation event dN_γ/dE), and c) on the spatial distribution of the DM within our halo. In this section we will focus on the astrophysical contribution, while incorporating particle physics and detector properties for the predictions of subhalo detectability in the following section.

2.1. *Simulations*

The "Via Lactea" simulations follow the formation and evolution of the dark matter substructure of a Milky-Way-scale halo in a cosmological volume. The first of these simulations (VL-I) consists of 234 million high resolution particles, covering the virial volume and its immediate surroundings of a $M_{200} = 1.77\times10^{12}\,M_\odot$ halo. With a particle mass of $\simeq 21,000\,M_\odot$, this simulation resolves around 10,000 subhalos within $r_{200} = 388$ kpc[1]. The global $z = 0$ properties of the host halo and the substructure population were presented in Diemand et al. (2007a), the joint temporal evolution of host halo and substructure properties was discussed in Diemand et al. (2007b), and an analysis of the shapes, alignment, and spatial distribution of the subhalos can be found in Kuhlen et al. (2007). Recently we have completed "Via Lactea II", the next generation of this series of simulations (Diemand et al. 2008). At a cost of over 1 million cpu-hours on Oak Ridge National Lab's *Jaguar* supercomputer, VL-II employs just over one billion $4,100\,M_\odot$ particles to model the formation of a $M_{200} = 1.93\times10^{12}\,M_\odot$ halo and its substructure. For this simulation we used for the first time a novel adaptive time-step method (Zemp et al. 2007), which assigns time-steps equal to 1/16 of the local dynamical time (but no shorter than 268,000 yr). This allows us to accurately resolve the density structure much farther into the central regions of the host halo. With VL-II we are able to resolve more than 50,000 individual subhalos within the host halo's $r_{200} = 402$ kpc. Roughly 2,000 of these are found within 50 kpc of the center, and 20 within the solar circle. For reference the parameters of these two simulations are summarized in Table 1. The calculations presented in this paper have been performed for both simulations, but the final results are based on the higher resolution VL-II.

Given the position of a fiducial observer, located 8 kpc from the host halo center, we bin up the sky into a grid of 2400×1200 pixels, equally spaced in longitude (ϕ) and in the cosine of the co-latitude ($\cos\theta$). This pixel size was chosen to approximate the best angular resolution of GLAST's LAT detector, equal to about 9 arcmin (see Section 3). Each pixel corresponds to a solid angle of $\Delta\Omega = (2\pi)/2400\times2/1200 = 4.363\times10^{-6}$ sr. We then calculate each particle's angular coordinates on the sky $(\phi_i, \cos\theta_i)$, and sum up the fluxes, $F_i = m_p\rho_i/4\pi d_i^2$, of all particles in a given pixel. Here d_i is the distance from the $i^{\rm th}$ particle to the observer, ρ_i is its density, measured over a 32 particle SPH-kernel, and we have approximated $\int\rho_i^2 dV$ as $m_p\rho_i$, which is appropriate for a collection of discrete simulated DM particles of mass m_p. In order to minimize shot noise arising from particle discreteness we smooth each particle's contribution using a projected SPH-kernel of angular width h_i/d_i, where h_i is half the radius encompassing all 32 neighboring particles. The resulting map is presented in the top left panel of Fig. 1 in units of GeV^2 kpc cm^{-6} sr^{-1} and depends only the choice of the observer's location and the dark matter distribution. The flux from only those particles belonging to subhalos is shown in the top right panel.

2.2. *Subhalo Boost Factor*

The hierarchical nature of CDM structure formation implies that substructure should be expected not only in the host halo, but also in individual subhalos. Indeed, in VL-II we are able to resolve some of these sub-subhalos in the most massive of our subhalos. In Diemand et al. (2008) we show that the mean abundance of sub-substructure is consistent with a scaled-down version of the VL-II host halo, i.e. once the sub-subhalos' $V_{\rm max}$'s are scaled by the $V_{\rm max}$ of *their* host subhalo, the cumulative $V_{\rm max}$-function ($N(>V_{\rm max})$) agrees with the overall subhalo $V_{\rm max}$-function. A density squared projection of four of the most massive subhalos is shown in Fig. 2. Only particles within the subhalo's outer radius $r_{\rm sub}$ have been included in the projection.[2] The subhalos' r_{1000}, the radius at which the mean enclosed density is equal to 1000 times the mean matter density of the universe, is overplotted with a dashed line.

Even with VL-II's impressive dynamical range of $\sim10^6$ in mass, however, we still resolve only a small fraction of the total expected DM substructure hierarchy. In principle this hierarchy could extend all the way down to the cut-off in the matter power spectrum, set by collisional damping and free streaming in the early universe (Green et al. 2005; Loeb & Zaldarriaga 2005). For WIMP dark matter, typical kinetic decoupling temperatures range from MeV to GeV, corresponding to cut-off masses of $m_0 = 10^{-12}$ to $10^{-4}\,M_\odot$ (Profumo et al. 2006), some 10 to 20 orders of magnitude below VL-II's mass resolution. Since the annihilation rate goes as density squared, any clumpiness will lead to an enhancement of the total luminosity compared to a smooth mass distribution.

[1] Note that we define r_{200} as the radius enclosing 200 times the *mean* density of the universe

[2] $r_{\rm sub}$ is defined here as the radius at which the total density becomes roughly constant.

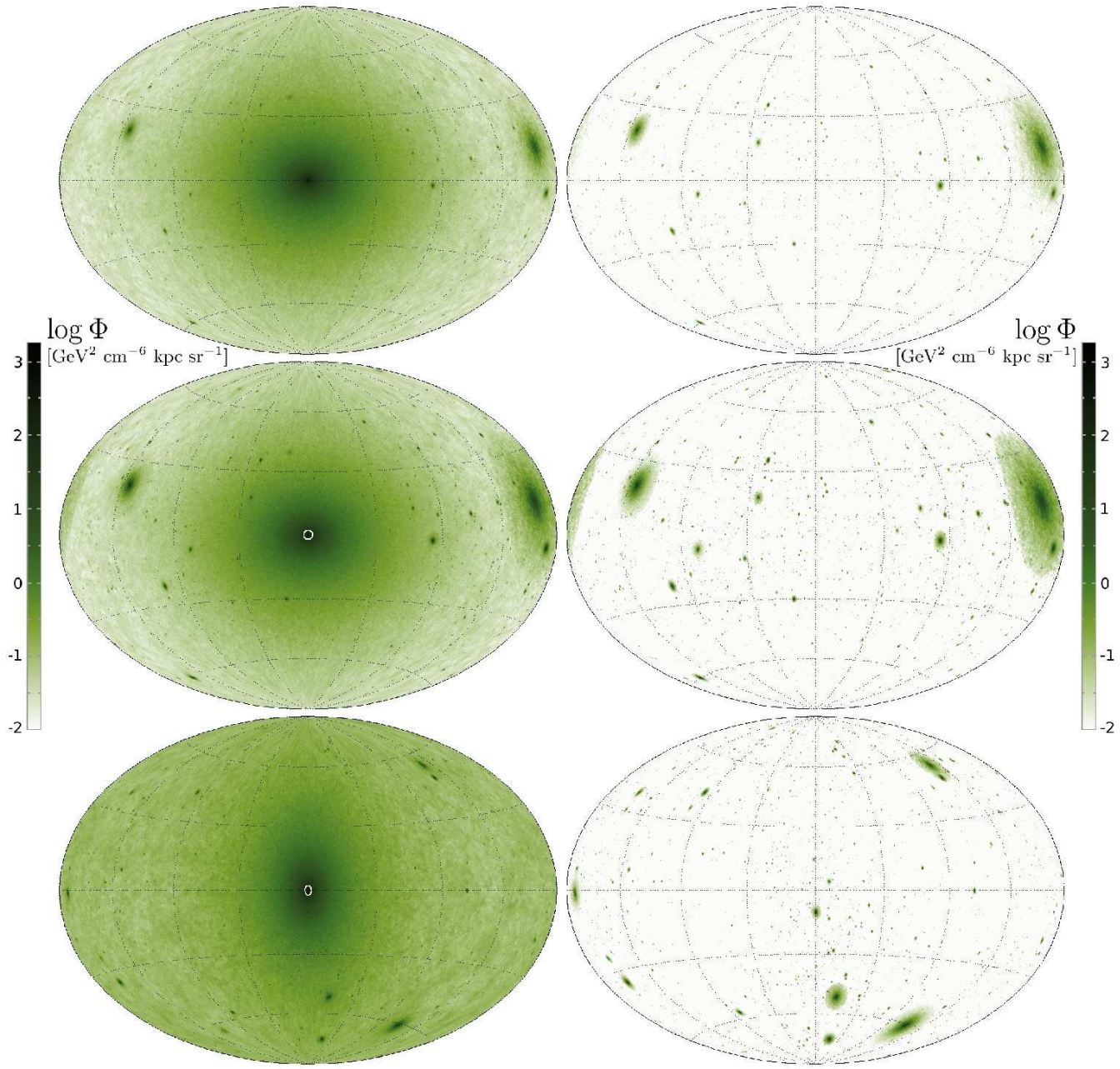


FIG. 1.— Allsky maps of the annihilation signal from VL-II, for an observer 8 kpc from the halo center along the host halo's intermediate principal axis (top two rows) and along its major axis (bottom row). The maps in the left panel show the total annihilation signal from all DM particles within r_{200}, in the right panel only the signal from subhalo particles. In the top row we show the uncorrected signal directly from the simulation, in the bottom two rows the halo center, indicated with a small white ellipse, has been replaced with an artificial $\rho \propto r^{-1}$ cusp, and a mass-dependent boost factor (for $m_0 = 10^{-6}\,\mathrm{M}_\odot$, $\alpha = 2.0$) has been applied to the subhalos.

The unresolved portion of the substructure hierarchy will thus lead to a boost in the true annihilation luminosity of individual subhalos, compared to the value determined directly from the numerical simulation. The magnitude of this boost will depend sensitively on the properties of the subhalo population, in particular on the slope and low mass cut-off of the subhalo mass function and on the subhalo concentration-mass relation. Our analytic boost factor model is based on the one presented in Strigari et al. (2007a). The true luminosity of a subhalo of mass M is given by

$$L(M) = [1 + B(M)]\,\tilde{L}(M), \tag{2}$$

where

$$\tilde{L}(M) \propto \int_V \rho^2_{\rm sub} dV = \sum_{r_i < r_{\rm sub}} \rho_i m_p \tag{3}$$

is the luminosity of the subhalo determined from all simulation particles within the subhalo's outer radius and ρ_i is the density of the $i^{\rm th}$ such particle. A subhalo's $B(M)$ can be calculated by integrating luminosities over its own

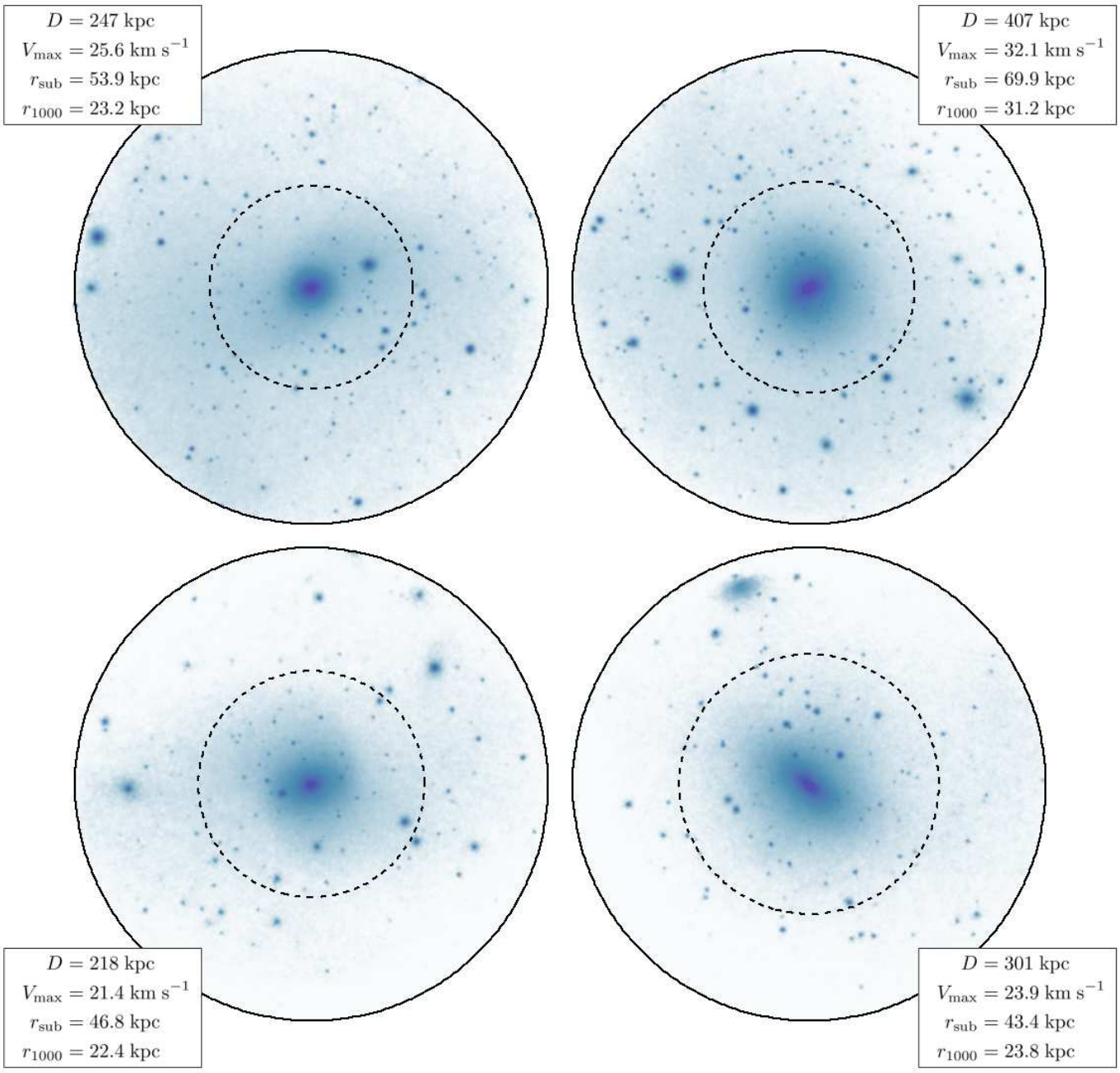


FIG. 2.— Sub-substructure in four of VL-II's most massive subhalos. Shown are projections of ρ^2 for all particles within a subhalo's outer radius $r_{\rm sub}$. The dashed circle indicates the subhalo's r_{1000}. The clumpy sub-substructure boosts the total annihilation luminosity of its host subhalo.

sub-subhalo population:

$$B(M) = \frac{1}{\tilde{L}(M)} \int_{m_0}^{m_1} \frac{dN}{dm} L(m) dm \quad (4)$$

$$= \frac{1}{\tilde{L}(M)} \int_{m_0}^{m_1} \frac{dN}{dm} \left[1 + B(m)\right] \tilde{L}(m) dm. \quad (5)$$

Here dN/dm is the sub-subhalo mass function, and the integration extends from m_0, the low mass cut-off of the substructure hierarchy, to an upper limit of $m_1 = \min\{10^6\,{\rm M}_\odot, 0.1{\rm M}\}$, such that only substructure below VL-II's resolution limit of $\sim 10^6\,{\rm M}_\odot$ contribute. For subhalos below $10^7\,{\rm M}_\odot$ we cap the integration at $0.1M$ under the assumption that efficient dynamical friction would have lead to the tidal destruction of larger sub-subhalos. For a power law substructure mass function $dN/dm = A/M(m/M)^{-\alpha}$, Eq. 5 becomes

$$B(M) = \frac{A}{\tilde{L}(M)} \int_{\ln m_0}^{\ln m_1} \left(\frac{m}{M}\right)^{1-\alpha} \left[1 + B(m)\right] \tilde{L}(m) d\ln m. \quad (6)$$

Motivated by our numerical simulations (Diemand et al. 2004a, 2007a) and semi-analytic studies (Zentner & Bullock 2003), we normalize the sub-subhalo mass function by setting the mass fraction in subclumps with masses $10^{-5} < m/M < 10^{-2}$ equal

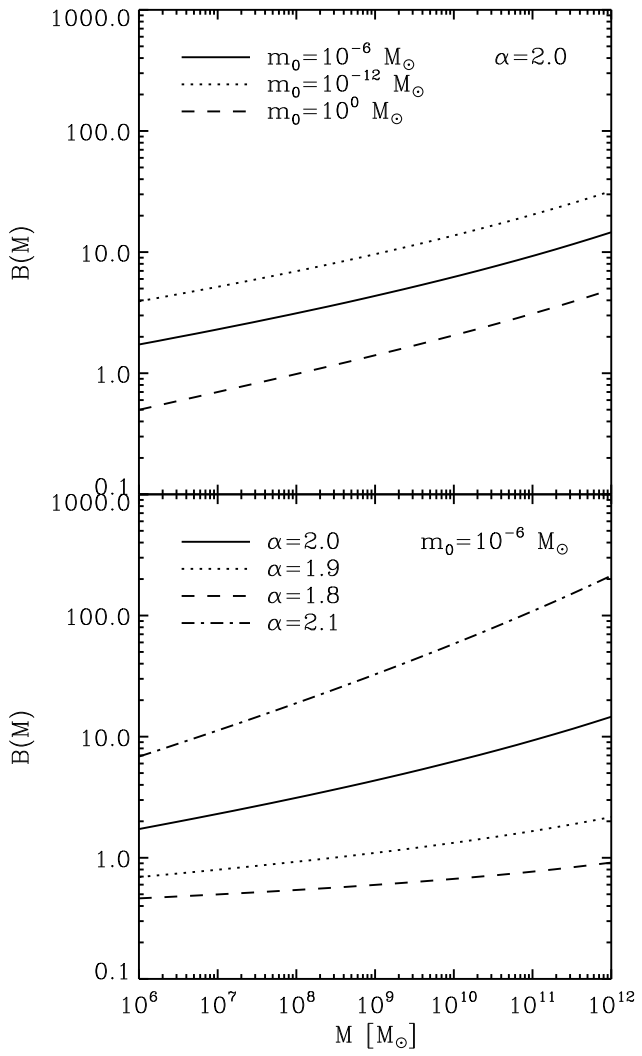


FIG. 3.— The annihilation luminosity boost factor due to substructure below VL-II's resolution limit versus subhalo mass, for different subhalo mass functions. *Top panel:* Dependence on the cutoff mass m_0 for slope $\alpha = 2.0$. *Bottom panel:* Dependence on α for $m_0 = 10^{-6}\,\mathrm{M}_\odot$.

to 10%.

For the determination of $\tilde{L}(M)$ we have assumed an NFW density profile, in which case the total annihilation luminosity of a halo of mass M and concentration $c = r_{\rm vir}/r_s$ is given by

$$\tilde{L}(M,c) \propto \rho_s^2 r_s^3 \propto M \frac{c^3}{f(c)^2}, \qquad (7)$$

where $f(c) = \ln(1+c) - c/(1+c)$. We use the Bullock et al. (2001) concentration-mass relation for field halos, albeit with a somewhat smaller value of the normalization, $K = 3.75$ (as suggested by Kuhlen et al. 2005; Macciò et al. 2007). For the cosmology used in the VL simulations and halos masses between 10^6 and $10^{10}\,\mathrm{M}_\odot$, the c(M) relation is approximately $c(M) \approx 18(M/10^8\,\mathrm{M}_\odot)^{-0.06}$, which corresponds to $\tilde{L}(M) \propto M^{0.87}$, i.e. the annihilation luminosity scales almost linearly with mass, in agreement with results from numerical simulations (Stoehr et al. 2003; Diemand et al. 2007a). Note that in our numerical simulations we find systematically higher subhalo concentrations closer to the host halo center. This trend does not affect the magnitude of the boost factor, but translates to a radial trend in subhalo luminosity (see Section 3.1).

Eq. 6 is solved numerically using the boundary condition $B(m_0) = 0$. The resulting relation is plotted in Fig. 3, for $\alpha = 2.0$ and different values of m_0 in the top panel, and for $m_0 = 10^{-6}\,\mathrm{M}_\odot$ and different values of α in the bottom panel. Overall we find relatively modest boost factors on the order of a few, ranging up to ~ 10 for the most massive subhalos. Generally more massive halos have larger boost factors, simply because their subhalo population covers more of the total subhalo hierarchy. For the same reason, smaller values of m_0 lead to larger boost factors. For $\alpha < 2.0$ $B(M)$ has a weaker mass dependence and is less sensitive to m_0, since in this case more massive halos are relatively more important. Our results are in agreement with the analytic upper limits of Strigari et al. (2007a) and the recent calculations of Lavalle et al. (2008).

A fit to the cumulative subhalo mass function in our simulations is consistent with $\alpha = 2$ (Diemand et al. 2007a), which implies equal mass in subhalos per decade of subhalo mass. However, fits to the differential mass function tend to favor slightly shallower slopes of $1.8-1.9$ (Stoehr et al. 2003; Madau et al. 2008), possibly because they are more sensitive to the lower mass end, where resolution effects may artificially flatten the slope. In this work we use $\alpha = 2.0$ and $m_0 = 10^6\,\mathrm{M}_\odot$ as our fiducial model, but present results for a range of different α and m_0.

2.3. *Central Flux Corrections*

The host halo center is another area where our simulation must be corrected to account for the artificially low density caused by the finite numerical resolution (Diemand et al. 2004b). Based on numerical convergence studies (Diemand et al. 2005a) we believe that we can trust the radial density profile of the VL-I host halo down to $r_{\rm conv} = 3.4\times10^{-3} r_{200} = 1.3$ kpc (Diemand et al. 2007a), corresponding to about 10° from the center. The higher mass resolution and improved time-step criterion in VL-II results in a much smaller convergence radius of $r_{\rm conv} = 380$ pc. The flux derived directly from the simulated particles in VL-II will thus only underestimate the true annihilation flux within the inner $\sim 2°$ from the center. An additional uncertainty arises from the fact that our purely collisionless DM simulation completely neglect the effect of baryons. While this is not a problem for the signal from individual subhalos, which are small enough that baryonic effects are likely negligible, the central region of our host halo most likely would have been affected by gas cooling, star formation, and stellar dynamical processes. It is not immediately obvious how such baryonic effects would alter the central DM distribution. Adiabatic contraction (Blumenthal et al. 1986; Gnedin et al. 2004a) would lead to a steepening of the central DM density profile at scales of a few kpc and below. A recent study of scaling relations in spiral galaxies, however, seems to favor models of spiral galaxy formation

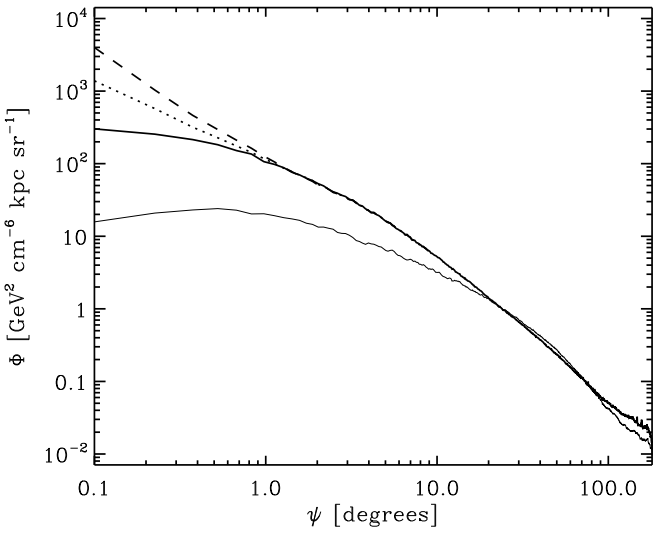


FIG. 4.— The gamma-ray intensity from DM annihilations in the smooth host halo versus the angle from the Galactic center, directly from the simulated VL-II particles (*thick solid line*), and with an artificial central cusp with central slope equal to 1.0 (*dotted line*) and 1.2 (*dashed line*). For comparison the smooth host halo flux from the VL-I simulation is overplotted (*lower thin solid line*).

without adiabatic contraction, and suggests that clumpy gas accretion might have reduced central DM densities (Dutton et al. 2007). Stirring by a stellar bar could also eject DM from the central regions (Weinberg & Katz 2007, and references therein). On much smaller scales (central few pc), the presence of a supermassive black hole (SMBH) would lead to the creation of an $r^{-1.5}$ minicusp (Gnedin & Primack 2004b). A SMBH binary, on the other hand, could have removed DM from the very center (Merritt et al. 2002).

Here we have attempted to correct for the artificially low central density by excising all simulated particles within $r_{\rm conv}$ and replacing them with an artificial cusp consisting of about 25 million 5 $M_\odot$ particles, distributed in an ellipsoid matched to the shape and density of the VL-II host halo at $r_{\rm conv}$, and extended inwards with a power law density profile. The resulting radial flux profile (excluding subhalos) is plotted in Fig. 4, for the uncorrected case and for central density slopes of -1 and -1.2.

Note that a similar correction should be applied to the centers of all the subhalos as well. This, however, is computationally very expensive, and we omit a direct correction of the particle distribution in favor of applying an *a posteriori* correction to the central pixel of each subhalo in the final allsky map. For each subhalo we estimate the central surface brightness according to

$$\Phi_c = \frac{1}{\Delta\Omega}\mathcal{F}_{\rm halo}(\rho_s, r_s, D), \tag{8}$$

where $\mathcal{F}_{\rm halo}$ is the flux from the central region subtended by solid angle $\Delta\Omega$ of a subhalo with NFW scale density ρ_s and scale radius r_s at a distance D (see Eq. A11). We estimate ρ_s and r_s from the measured values of $V_{\rm max}$ and $r_{\rm Vmax}$ according to the relations

$$r_s = \frac{r_{\rm Vmax}}{2.163} \tag{9}$$

$$\rho_s = \frac{4.625}{4\pi G}\left(\frac{V_{\rm max}}{r_s}\right)^2, \tag{10}$$

which hold for an NFW density profile. If the central pixel of a subhalo has $\Phi < \Phi_c$, we set it equal to Φ_c. Note that we first apply the boost factor correction to all particles of a given subhalo, and then apply this flux correction to the central pixel. We only correct the central pixel, so subhalos for which r_s subtends more than one pixel (1.7% of all VL-II subhalos) will not be fully corrected.

2.4. *Corrected Allsky Maps*

In Fig. 1 we show both unmodified and corrected DM annihilation flux allsky maps. While the topmost row shows the signal as calculated directly from the numerical simulation, in the center row the subhalo particle fluxes have been boosted by $B(M)$, assuming $(\alpha, m_0) = (2.0, 10^{-6})$, the central pixel flux correction has been applied, and the central region of the host halo has been replaced with an artificial density cusp of slope -1. In these two rows the observer is located at 8 kpc along the intermediate axis of the host halo ellipsoid. In the panels on the right hand side, we show only the fluxes from particles belonging to subhalos, i.e. within a given subhalo's outer radius. The addition of a substructure boost factor lifts the brightness of a number of subhalos over the level of the diffuse host halo flux. The bottom panel shows the corrected case for an observer placed at 8 kpc along the major axis of the host halo. In this case the observer is deeper inside the host halo mass distribution, and the resulting diffuse host halo flux dominates over most of the subhalos.

3. SUBHALO DETECTABILITY

In order to make predictions for the number of detectable subhalos, we must convert the simulation fluxes presented in Section 2 into actual gamma-ray photon fluxes and compare these to the expected background signal. Following previous work (Stoehr et al. 2003), we define for each subhalo in our allsky map a "detection significance"

$$\mathcal{S} = \frac{\sum_i N_{s,i}}{\sqrt{\sum_i N_{b,i}}}, \tag{11}$$

where $N_{s,i}$ and $N_{b,i}$ are the number of source and background gamma-rays received on a given pixel, and the sums are over all pixels with signal-to-noise $(N_{s,i}/N_{b,i}^{1/2})$ greater than unity covered by a subhalo. For this purpose we must make assumptions about the observation (the detector's effective area and angular resolution as a function of energy, the exposure time and energy threshold), the astrophysical backgrounds (extragalactic and Galactic), and, most importantly, the nature of the DM particle (its mass and annihilation cross section, the annihilation spectrum).

Here we adopt parameters appropriate for a GLAST observation with the Large Area Telescope (LAT): an exposure time of $\tau_{\rm exp} = 2$ years, the expected energy-dependent effective area $A_{\rm eff}(E)$, and an energy threshold of $E_{\rm th} = 3.0$ GeV, above which the flux-weighted

mean angular resolution

$$\langle \Delta\theta \rangle \equiv \frac{\int_{E_{\rm th}}^{\infty} \Delta\theta(E)\ A_{\rm eff}(E)\ (dN_\gamma/dE)\ dE}{\int_{E_{\rm th}}^{\infty} A_{\rm eff}(E)\ (dN_\gamma/dE)\ dE} \qquad (12)$$

is equal to 9 arcmin. The functional form of $A_{\rm eff}(E)$ and $\Delta\theta(E)$ was obtained from the GLAST LAT Performance webpage[3].

3.1. *Backgrounds*

The annihilation signal from individual extended subhalos must compete with a number of diffuse gamma-ray backgrounds, of both astrophysical and particle physics origin. The Energetic Gamma Ray Experiment Telescope (EGRET) aboard the Compton Gamma Ray Observatory satellite conducted a gamma-ray allsky survey in the 1990's, detecting a diffuse background consisting of an isotropic extragalactic (Sreekumar et al. 1998) as well as a Galactic component (Hunter et al. 1997). The extragalactic component is probably dominated by unresolved blazars (Stecker & Salamon 1996; Giommi et al. 2006), although star-bursting galaxies and galaxy clusters might add a substantial contribution (Chiang & Mukherjee 1998; Dermer 2007). The spectrum of this extragalactic background is well described by a power-law photon spectrum in the 30 MeV to 100 GeV energy range (Sreekumar et al. 1998):

$$\Phi_{\rm eg} = (7.32 \pm 0.34) \times 10^{-9} \quad {\rm MeV}^{-1}{\rm cm}^{-2}{\rm s}^{-1}{\rm sr}^{-1} \left(\frac{E}{451{\rm MeV}}\right)^{(-2.10\pm0.03)} . \qquad (13)$$

The diffuse Galactic gamma-ray background is produced by energetic interactions of cosmic ray nucleons with interstellar medium (ISM) atoms through neutral pion production, as well as from energetic electrons by inverse Compton upscattering of lower energy photons and bremsstrahlung. Modeling this background under the assumption that the locally measured electron and proton energy spectra are representative of the Galaxy as a whole ("conventional model") underpredicts the flux in the measured EGRET spectrum above 1 GeV by about a factor of two (Hunter et al. 1997). Strong et al. (2004a) provide an explanation for this "GeV excess" by modeling cosmic ray propagation within the Galaxy, allowing for mild departures in the electron and nucleon spectra from the conventional model, and using a cosmic ray source distribution based on the observed distribution of pulsars and supernova remnants in conjunction with a variable CO-to-H_2 conversion factor (Strong et al. 2004b). This "optimized model" emphasizes the importance of inverse Compton emission and is able to reproduce the EGRET observations in all directions of the sky. Here we have employed the GALPROP[4] (v50p) cosmic ray propagation code (Strong & Moskalenko 1998; Moskalenko et al. 2002, and references therein) to calculate an "optimized model" allsky map of the gamma ray emissivity due to cosmic ray interactions with the Galactic ISM. We have limited the pixel size of this map to 0.5°, corresponding to the angular resolution of the HI and CO surveys used in GALPROP.

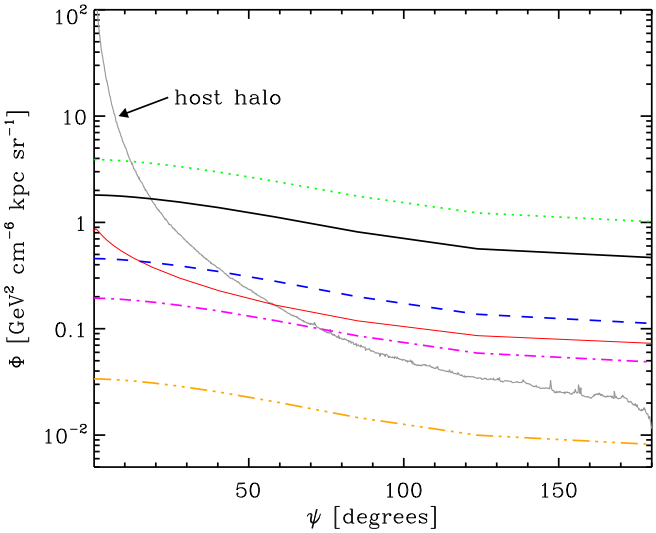


FIG. 5.— Diffuse flux due to undetectable subhalos as a function of angle ψ from the Galactic center, for a number of different subhalo mass functions. The thick lines show models with an anti-biased radial distribution, concentrations increasing towards the host center, and different values of the mass function slope α and low mass cutoff m_0: $(\alpha, m_0/{\rm M}_\odot) = (2.0, 10^{-6})$ (*solid*), $(2.0, 10^{-12})$ (*dotted*), $(2.0, 1)$ (*dashed*), $(1.9, 10^{-6})$ (*dot-dashed*), $(1.8, 10^{-6})$ (*triple-dot-dashed*). The thin solid line represents the original Pieri et al. (2008) model ($B_{\rm ref,z0}$), with $\alpha = 2.0$, $m_0 = 10^{-6}\,{\rm M}_\odot$, an un-biased radial distribution, and no radial concentration dependence. The flux from the smooth host halo is overplotted with the grey line, see Fig. 4.

In addition to these astrophysical backgrounds, individual detectable subhalos must outshine DM annihilations from the smooth host halo as well as the background from the population of individually undetectable subhalos (Pieri et al. 2008). Note that these undetectable subhalos do not simply uniformly boost the flux from the smooth host halo. Tidal disruption of satellites is more effective close to the host halo center, leading to a spatial distribution of subhalos that is antibiased with respect to the host halo mass distribution (Kuhlen et al. 2007; Madau et al. 2008). The resulting background will have a shallower angular dependence than the smooth host halo signal, and can dominate it at large angular distances from the center.

To determine the magnitude and angular dependence of this background we repeat the calculation presented in Pieri et al. (2008), with three important differences. Firstly, we use an antibiased subhalo spatial distribution for which $n_{\rm sub}(r)/\rho_{\rm host}(r) \propto r$ (see Kuhlen et al. 2007), as opposed to one that follows the host halo mass distribution down to some hard cut-off $r_{\rm min}(M)$ as in Pieri et al. (2008). Secondly, we allow a range of values of the subhalo mass function slope α and cutoff mass m_0. This can make a big difference, since by number the population of individually undetected subhalos is dominated by objects with masses close to m_0. Lastly, we include a radial dependence in the subhalo mass-concentration relation, motivated by numerical simulations which tend to find higher concentrations for subhalos closer to the

[3] http://www-glast.slac.stanford.edu/software/IS/glast_lat_performance.htm

[4] available from `http://galprop.stanford.edu/web_galprop/galprop_home.html`

TABLE 2
Subhalo Mass Function Models

α	m_0 ($M_\odot$)	$N_{\rm tot}$	$M_{\rm tot}$ ($M_\odot$)	$f_{\rm tot}$	$M_{\rm u}$ ($M_\odot$)	$f_{\rm u}$
2.0	10^{-6}	2.5×10^{16}	9.3×10^{11}	0.53	7.0×10^{11}	0.40
1.9	10^{-6}	9.2×10^{14}	3.2×10^{11}	0.19	1.2×10^{11}	0.070
1.8	10^{-6}	3.3×10^{13}	2.1×10^{11}	0.12	3.3×10^{10}	0.018
2.0	1	2.5×10^{10}	5.8×10^{11}	0.33	3.5×10^{11}	0.20
2.0	10^{-12}	2.5×10^{22}	1.3×10^{12}	0.73	1.0×10^{12}	0.60

Note. — The total number ($N_{\rm tot}$), mass ($M_{\rm tot}$), and mass fraction ($f_{\rm tot} = M_{\rm tot}/M_{\rm halo}$) by extrapolation of the subhalo mass function with slope α and cutoff m_0, normalized to give $f = 0.1$ in the interval $10^{-5} < M/M_{\rm halo} < 10^{-2}$. $M_{\rm u}$ and $f_{\rm u}$ are the mass and mass fraction of all subhalos below VL-II's resolution limit of $\sim 10^6\,M_\odot$.

host halo center (Diemand et al. 2007b, 2008),

$$c_0^{\rm sub}(M,R) = c_0^{\rm B01}(M)\left(\frac{R}{r_{200}}\right)^{-0.286}, \qquad (14)$$

where $c_0^{\rm B01}(M)$ is the median concentration of subhalo of mass M, as given by the Bullock et al. (2001) model for field halos. With this scaling, subhalos at $R_\odot$ are three times as concentrated as field halos. We also include a log-normal scatter around this median, with width $\sigma_{\log_{10}c} = 0.14$ (Wechsler et al. 2002). In Fig. 5 we present the resulting background flux as a function of angle from the halo center, and also show the effects of our modifications on the original Pieri et al. (2008) prescription (using their $B_{\rm ref,z0}$ model). A more detailed explanation of our calculation of this background is included in the Appendix A.

We find that our use of an anti-biased radial distribution leads to a diffuse subhalo flux that is almost independent of the viewing direction. The median galactocentric distance of a subhalo (i.e. the radius enclosing half of all subhalos) is about 200 kpc in the anti-biased case, but only 100 kpc for the unbiased distribution used by Pieri et al. (2008). The fraction of subhalos within 8 kpc (within $r_s^{\rm VL-II} = 21$ kpc) is 7×10^{-4} (0.01) in the anti-biased case, and 0.02 (0.1) for the unbiased distribution. In the unbiased case, subhalos within 8 kpc of the Galactic center contribute about 90% of the subhalo diffuse flux towards the Galactic center, whereas they only make up 40% of the flux in the anti-biased case. The shift towards larger distances also leads to an overall reduction in the amplitude of the flux.

The final background considered here is due to annihilations from the smooth host halo. For this component we simply use the angular flux distribution calculated from all simulated particles that don't belong to any subhalos. Since higher numerical resolution would have resolved some of this DM mass into individual subhalos, whose contribution we have accounted for above, we uniformly reduce the smooth halo flux by a factor $(1 - f_u)$, where f_u is the mass fraction below $10^6\,M_\odot$ (last column in Table 2).

3.2. *Particle Physics Parameters*

The particle physics dependence of the annihilation signal (Eq. 1) enters through three factors: M_χ, the mass of the DM particle, $\langle\sigma v\rangle$, the thermally averaged velocity-weighted annihilation cross section, and dN_γ/dE, the photon spectrum resulting from a single annihilation event. The physical nature of DM is currently unknown, and a plethora of particle physics models have been proposed to explain its existence. It should be noted that not all of these models result in a DM particle capable of annihilating, but those models are not of interest for the present work. Instead we consider here only the class of models in which the DM is a weakly interacting massive particle (WIMP), such as the neutralino in supersymmetric extensions of the standard model or Kaluza-Klein excitations of standard model fields in models with universal extra dimensions (for a recent review of particle DM theories, see Bertone et al. 2005a).

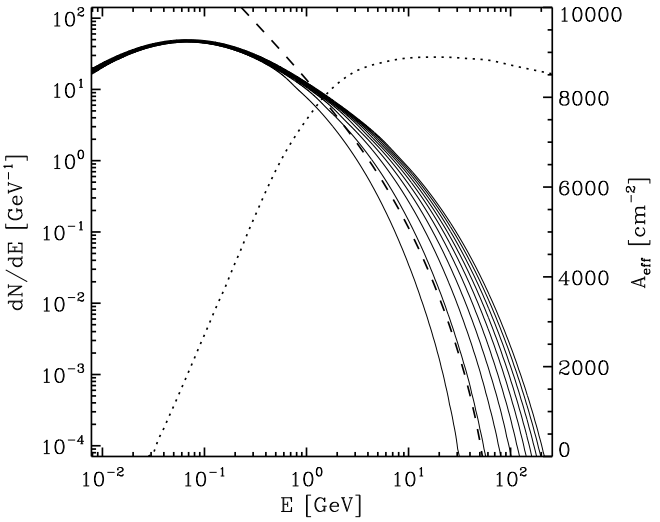


Fig. 6.— The gamma-ray spectrum dN/dE resulting from WIMP annihilations into $b\bar{b}$ quark pairs, calculated with DarkSUSY (Gondolo et al. 2004), for M_χ between 50 and 500 GeV in increments of 50 GeV. The dashed line shows the Fornengo et al. (2004) fitting function for $M_\chi = 100$ GeV and the dotted line the expected effective area of the GLAST/LAT detector (right abscissa).

For any given class of model it is possible to determine a range of M_χ and $\langle\sigma v\rangle$ resulting in a current relic DM density that is consistent with the WMAP measurement of $\Omega_\chi h^2 = 0.1105^{+0.0039}_{-0.0038}$ (Spergel et al. 2007). Typical values for M_χ are 50 GeV up to ~ 1 TeV, and a simple estimate of the cross section is $\langle\sigma v\rangle = 3\times10^{-27}{\rm cm^3 s^{-1}}/\Omega_\chi h^2 \approx 3\times10^{-26}$ cm^3 s^{-1}(Jungman et al. 1996). However, this naive relation can fail badly (Profumo 2005), and a much wider range of cross sections, up to $\langle\sigma v\rangle \sim 10^{-24}$ cm^3 s^{-1} for $M_\chi < 200$ GeV (e.g. Fig.17 in Colafrancesco et al. 2006), should be considered viable. In this work we consider values of M_χ from 50 to 500 GeV, and $\langle\sigma v\rangle$ from 10^{-26} to 10^{-25} cm^3 s^{-1}.

WIMP DM particles can annihilate into a range of different particle pairs, including quarks, leptons (e.g. τ's), gauge bosons (Z^0, $W^\pm$), gluons, and Higgs particles. The subsequent decay and hadronization of the annihilation products leads to a spectrum of gamma-rays, mostly resulting from the decay of π^0 mesons. The shape of this spectrum is almost independent of the annihilation branch (with the exception of the τ branch, which has a harder spectrum, Cesarini et al. 2004; Fornengo et al. 2004), and can be calculated using Monte-Carlo simulation, for example with the PYTHIA

package (Sjöstrand et al. 2001). Above $x = (E_\gamma/M_\chi) = 0.01$ the spectrum is typically well fit by a function of the form $\alpha_0 x^{3/2}\exp(-\alpha_1 x)$, with (α_0, α_1) dependent on the final state (Bergström et al. 1998; Koushiappas et al. 2004; Fornengo et al. 2004). GLAST has non-negligible sensitivity down to $\sim$ 0.1GeV ($x < 0.01$), where the spectrum has turned over and the $x^{3/2}$ dependence is no longer a good match. Here we calculate dN/dE assuming a 100% branching ratio into $b\bar{b}$ quarks (Baltz et al. 2007; Pieri et al. 2008) and calculate the spectrum directly using the `DarkSUSY` code (Gondolo et al. 2004). Annihilation into two photons or a photon and a Z^0, resulting in a monochromatic gamma-ray line signal, is also possible, but is one-loop suppressed (Bergström & Ullio 1997) and we do not include such channels here. Fig. 6 shows the $b\bar{b}$ spectrum for M_χ between 50 and 200 GeV, together with the Fornengo et al. (2004) fitting function and the GLAST/LAT $A_{\rm eff}(E)$. For $M_\chi = 100$ GeV, this spectrum results in 32.6, 13.4, and 4.58 gamma-rays per annihilation above 0.1, 1.0, and 3.0 GeV, respectively.

Recently Bringmann et al. (2008) presented new calculations of the gamma-ray spectrum from DM annihilation, including electromagnetic radiative corrections to all leading annihilation processes. In some cases the inclusion of internal bremsstrahlung (IB) photons leads to large enhancements of the gamma-ray fluxes, and also sharpens the spectral feature at the mass of the DM particle. Above energies of $0.6M_\chi$, IB photons typically increase the gamma-ray flux by no more than a factor of two over the range of M_χ considered here. For the much lower energy threshold of 3 GeV employed in this study, the enhancement from IB photons is negligible, and thus we have not included IB photons here.

3.3. *EGRET Constraints*

Given the theoretically motivated modifications and additions to the simulated flux distribution discussed in the previous sections, we must ask whether our models still satisfy existing constraints from EGRET on the diffuse gamma-ray flux as well as limits on a Galactic center gamma-ray point source.

Integrating Eq. 13 from 30 MeV to 10 GeV, we obtain a specific intensity of 5.91×10^{-5} cm^{-2} s^{-1} sr^{-1} for the extra-galactic background in the EGRET energy range. Over this same energy range, DM annihilations result in 30-50 gamma rays per event for $M_\chi = 50 - 500$ GeV(see Section 3.2). The diffuse flux plotted in Fig. 5 can thus be converted to units of cm^{-2} s^{-1} sr^{-1} by multiplying by $(3.09 \times 10^{21}\mathrm{cm/kpc}) \times (30 - 50) \times \langle\sigma v\rangle/M_\chi^2$. Even the strongest diffuse background model considered here, $(\alpha, m_0/\,\mathrm{M}_\odot) = (2.0, 10^{-12})$, remains below the EGRET extragalactic background for $\langle\sigma v\rangle/M_\chi^2 < 10^{-28}$ cm^3 s^{-1} GeV^{-2}, i.e. over the full range of M_χ and $\langle\sigma v\rangle$ that we consider in the following analysis.

Hooper & Dingus (2004) performed a re-analysis of the EGRET Galactic center data with an improved energy dependent point spread function and found no evidence of a point source at the location of Sag A*. For M_χ between 50 and 500 GeV they determined a 95% confidence upper limit of $\sim 10^{-8}$ cm^{-2} s^{-1} for gamma rays above 1 GeV. The total flux from the innermost 30 arcmin (EGRET's angular resolution) from a central cusp matched to VL-II's density profile at $r_{\rm conv}$ is equal to 5.7×10^{-2} GeV^2 kpc cm^{-6} for a slope of -1.0. In the energy range from 1 to 30 GeV, DM annihilations produce $8 - 33$ gamma rays per event for $M_\chi = 50 - 500$ GeV, and the central flux exceeds the EGRET limit if $\langle\sigma v\rangle > 4.1 \times 10^{-26}(M_\chi/100\,\mathrm{GeV})^{1.41}$ cm^3 s^{-1}. Most of the parameter space we considered here satisfies this limit, but models with $M_\chi < 80$ GeV and $\langle\sigma v\rangle = 3\times10^{-26}$ cm^3 s^{-1} violate it. For an inner slope of -1.2 the constrait is stronger, and the EGRET limit is already exceeded if $\langle\sigma v\rangle > 1.5\times10^{-26}(M_\chi/100\,\mathrm{GeV})^{1.41}$ cm^3 s^{-1}. In this case a DM particle mass greater than 170 GeV (for $\langle\sigma v\rangle = 3 \times 10^{-26}$ cm^3 s^{-1}) would be required in order to remain below the EGRET point source limit. For the uncorrected central flux, which may in fact be closer to reality if dynamical processes have removed a significant amount of DM from the Galactic center, the limit is relaxed to $\langle\sigma v\rangle > 1.5 \times 10^{-25}(M_\chi/100\,\mathrm{GeV})^{1.41}$ cm^3 s^{-1}, in which case all models considered in this work would satisfy the limit.

3.4. *Detectable subhalos*

We have now assembled all necessary ingredients to convert our simulated particle distribution into a quantitative prediction for the number of subhalos detectable with GLAST. To recap: N_s, the expected number of gamma-rays from a subhalo in one GLAST 9 arcmin "pixel", is calculated by summing $B(M)\rho_i m_p/(4\pi d_i^2)$ over all the subhalo's particles falling within the pixel and multiplying by $\tau_{\rm exp}\langle\sigma v\rangle/(2M_\chi^2)\int_{E_{\rm th}}^{M_\chi} dN_\gamma/dE\, A_{\rm eff}(E)\, dE$. The total signal from a subhalo is obtained by summing N_s over all $S/N > 1$ pixels covered by the subhalo. This flux is then compared to $\sqrt{\sum N_b}$, the square root of the expected number of background photons, made up of an isotropic extragalactic astrophysical component (as measured by EGRET), an astrophysical Galactic background (calculated with GALPROP), and two diffuse DM annihilation backgrounds, one from undetectable subhalos and one from the smooth host halo. The resulting detection significance $\mathcal{S} = \sum N_s/\sqrt{\sum N_b}$ depends critically on the mass of the DM particle (smaller M_χ is better) and on its annihilation cross section (larger $\langle\sigma v\rangle$ is better). At fixed M_χ and $\langle\sigma v\rangle$, $\mathcal{S}$ depends on the normalization, the slope α, and the low mass cut-off m_0 of the subhalo mass function through the calculation of the boost factor and the two diffuse annihilation backgrounds. Note that changes in α and m_0 affect $\mathcal{S}$ in opposite ways: increasing the abundance of subhalos below VL-II's resolution limit, by increasing α or lowering m_0, raises the boost factor (good for detection) as well as the background from undetectable subhalos (bad for detection).

Due to departures from spherical symmetry in the host halo mass and subhalo spatial distribution (Kuhlen et al. 2007), the number of detectable subhalos will depend on the observer position. For an observer located at 8 kpc along the major axis of the host halo ellipsoid the diffuse host halo background will be higher than for an observer at the same distance along the minor axis (Calcáneo-Roldán & Moore 2000). Individual bright subhalos may also become undetectable from certain vantage points, if they fall behind the Galactic disk

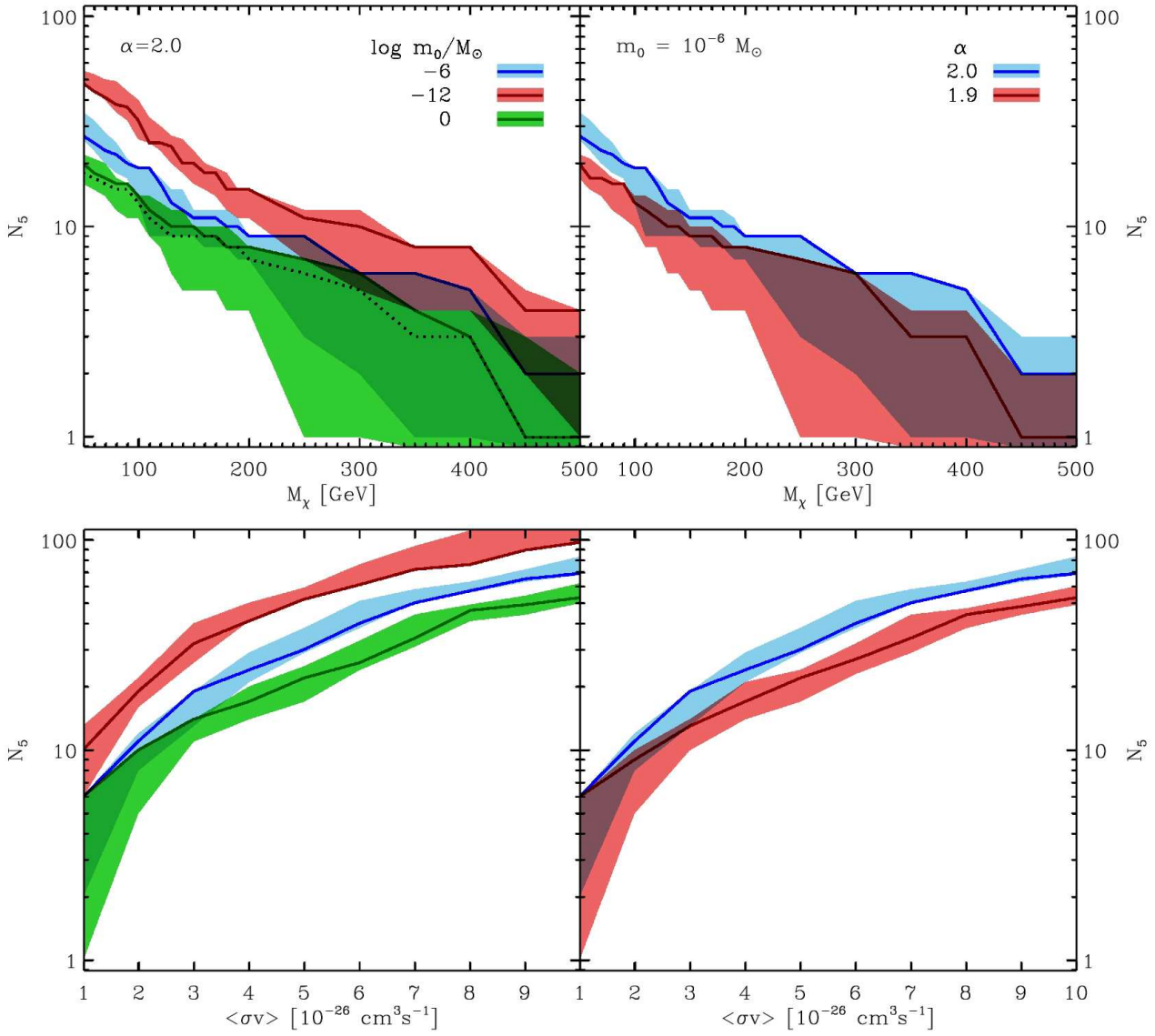


FIG. 7.— N_5, the number of simulated subhalos exceeding $\mathcal{S} = 5$, as a function of the DM particle mass M_χ for $\langle\sigma v\rangle = 3 \times 10^{-26}$ cm^3 s^{-1} (*top*) and the cross section $\langle\sigma v\rangle$ for $M_\chi = 100$ GeV (*bottom*). Dependence on the subhalo mass function cutoff mass m_0 for slope $\alpha = 2.0$ (*left*) and on α for $m_0 = 10^{-6}\,\mathrm{M}_\odot$ (*right*). The $\alpha = 1.8$ case is almost identical to $\alpha = 1.9$ and has been omitted from this plot. The shaded regions indicate the range of N_5 for ten randomly chosen observer locations and the solid lines refer to an observer placed along the intermediate axis of the host halo ellipsoid. The dotted line is the case without a boost factor.

or center for example. For these reasons we have performed our analysis for ten randomly drawn observer positions, in addition to our fiducial observer located along the host halo intermediate axis. Our results are presented in Fig. 7, where we plot N_5, the number of VL-II subhalos exceeding $\mathcal{S} = 5$, as a function of M_χ and $\langle\sigma v\rangle_{-26} = \langle\sigma v\rangle/(10^{-26}$ cm^3 s$^{-1})$, for different choices of α and m_0.

We find that N_5 ranges from a few up to multiple tens over the range of M_χ and $\langle\sigma v\rangle$ we have considered. In our fiducial model, $(M_\chi/\mathrm{GeV}, \langle\sigma v\rangle_{-26}, \alpha, m_0) = (100, 3, 2.0, 10^{-6})$, an observer positioned along the host halo's intermediate axis would be able to detect $N_5 = 19$ subhalos. For the set of ten randomly placed observers we find a range of N_5 from 13 to 19. Lowering m_0 from $10^{-6}\,\mathrm{M}_\odot$ to $10^{-12}\,\mathrm{M}_\odot$, the smallest value found by Profumo et al. (2006), results in a factor ~ 2 increase in N_5. In this case, assuming $\alpha = 2.0$, more than ten subhalos should be detectable even with M_χ as high as 300 GeV (for $\langle\sigma v\rangle_{-26} = 3$) or $\langle\sigma v\rangle$ as low as 10^{-26} cm^3 s^{-1} (for $M_\chi = 100$ GeV). If, on the other hand, no subhalos exist with masses less than $1\,\mathrm{M}_\odot$, then N_5 drops below 10 at $M_\chi \approx 160$ GeV (for $\langle\sigma v\rangle_{-26} = 3$) or $\langle\sigma v\rangle_{-26} \approx 2$ (for $M_\chi = 100$ GeV). Reducing α below the critical value of 2.0 suppresses N_5 by about a factor of 2/3. At a fiducial value of $(M_\chi, \langle\sigma v\rangle_{-26}) = (100, 3)$ we find $N_5 = 13 - 19$, $26 - 40$, $11 - 14$, $10 - 14$, and $9 - 14$ for $(\alpha, m_0) = (2.0, 10^{-6})$,

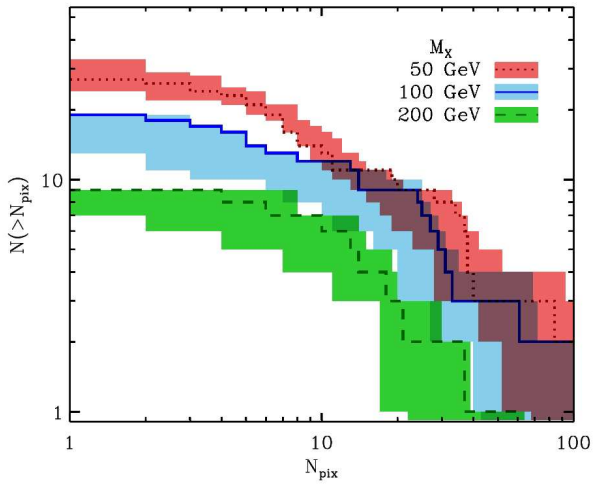


FIG. 8.— The number of detectable ($\mathcal{S} = 5$) subhalos with more than $N_{\rm pix}$ detectable pixels versus $N_{\rm pix}$, for three different choices of M_χ (assuming $\langle\sigma v\rangle = 3 \times 10^{-26}$ cm^3 s^{-1}). The shaded regions show the range of $N(> N_{\rm pix})$ for ten randomly chosen observer locations and the solid lines refer to an observer placed along the intermediate axis of the host halo ellipsoid.

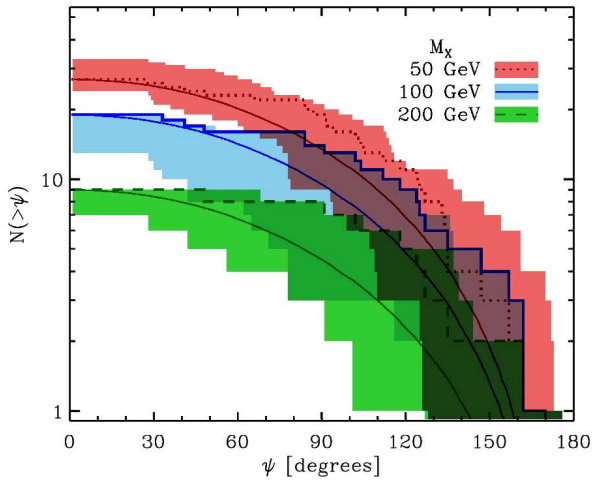


FIG. 9.— The cumulative angular distribution of detectable ($\mathcal{S} > 5$) subhalos, for three different choices of M_χ (assuming $\langle\sigma v\rangle = 3 \times 10^{-26}$ cm^3 s^{-1}). ψ is the angle from the direction of the host center to the brightest pixel in each subhalo. The shaded regions show the range of $N(> \psi)$ for ten randomly chosen observer locations and the solid lines refer to an observer placed along the intermediate axis of the host halo ellipsoid. The thin solid line represents an isotropic distribution normalized to the fiducial observer's location.

$(2.0, 10^{-12})$, $(2.0, 10^{0})$, $(1.9, 10^{-6})$, and $(1.8, 10^{-6})$, respectively. In the most favorable case considered here, $(M_\chi/\mathrm{GeV}, \langle\sigma v\rangle_{-26}, \alpha, m_0) = (100, 10, 2.0, 10^{-12})$, the number of detectable subhalos exceeds 100. The dependence of N_5 on m_0 and α is primarily driven by their effect on the boost factor: lowering the abundance of DM subhalos below VL-II's resolution limit reduces the boost factor and lowers N_5. For comparison we have also plotted results without a boost factor for the $(\alpha, m_0) = (2.0, 10^{-6})$ case. This case is similar to the $m_0 = 1\,\mathrm{M}_\odot$ case, and even without invoking such a sub-substructure boost factor multiple subhalos should be bright enough for detection for most of the parameter space probed here.

The set of models we have considered includes a model similar to the one recently proposed by Hooper et al. (2007) to explain the excess microwave emission around the Galactic center measured by WMAP (so-called "WMAP haze", Finkbeiner 2004). Hooper et al. (2007) showed that the intensity and angular distribution of the WMAP haze can be modeled as synchrotron emission from relativistic electrons and positrons generated in dark matter annihilations, assuming a cusped central DM density profile of slope -1.2, a DM particle mass of ~ 100 GeV, and an annihilation cross section of $\langle\sigma v\rangle = 3 \times 10^{-26}$ cm^3 s^{-1}. If this explanation for the WMAP haze turns out to be correct, we predict that GLAST should be able to detect about 15 subhalos.

In Fig. 8 we present the cumulative size distributions of all detectable subhalos, for $M_\chi = 50$, 100, and 200 GeV at fixed $\langle\sigma v\rangle = 3{\times}10^{-26}$ cm^3 s^{-1}. The size here is defined as the number of $S/N > 1$ pixels ($N_{\rm pix}$) contributing to the total subhalo signal exceeding the detection threshold of $\mathcal{S} = 5$. Recall that we have matched the pixel size to GLAST's angular resolution of 9 arcmin, such that each pixel corresponds to a solid angle of 4.363×10^{-6}sr. Again we plot distributions for the fiducial observer on the host halo's intermediate axis as well as the minimum and maximum over all ten randomly drawn observer positions. Detectable subhalos are typically extended, with a median of $N_{\rm pix}$ of 13. Only about 5% are detected in only one pixel. This should aid in discriminating between subhalos lit up by DM annihilation and conventional astrophysical sources (e.g. gamma-ray pulsars) which will often appear as point sources (Baltz et al. 2007).

The angular distribution of detectable subhalos is shown in Fig. 9, where we plot the cumulative number of detectable subhalos more than ψ degrees from the direction towards the host center. For the fiducial observer we have overplotted an isotropic distribution (thin solid line), in which detectable subhalos are uniformly distributed over the whole sky. The actual distribution indicates a slight excess at large angles compared to an isotropic distribution. However, a KS test shows that this discrepancy is not statistically significant. For only two of all eleven observer positions can the null hypothesis of an isotropic distribution be rejected at more than 90% confidence, and we conclude that the distribution of detectable sources on the sky is consistent with isotropy.

Next we consider the differential distribution of the detection significance $\mathcal{S}$, $V_{\rm max}$, and the distance to the observer, of the subset of detectable subhalos, see Fig. 10. In order to obtain better statistics for this analysis we chose a slightly higher cross section of $\langle\sigma v\rangle = 5 \times 10^{-26}$ cm^3 s^{-1}, resulting in 51, 29, and 12 detectable subhalos for $M_\chi = 50$, 100, 200 GeV, respectively. The histograms represent the results for the fiducial observer position and the error bars indicate the range of values for the 10 randomly drawn positions.

The $\mathcal{S}$ distribution is slightly peaked towards lower $\mathcal{S}$ values, with about two thirds of all detectable subhalos having $\mathcal{S} < 10$. About 10% of subhalos should be detectable at very high significances, with $\mathcal{S}$ exceeding 25.

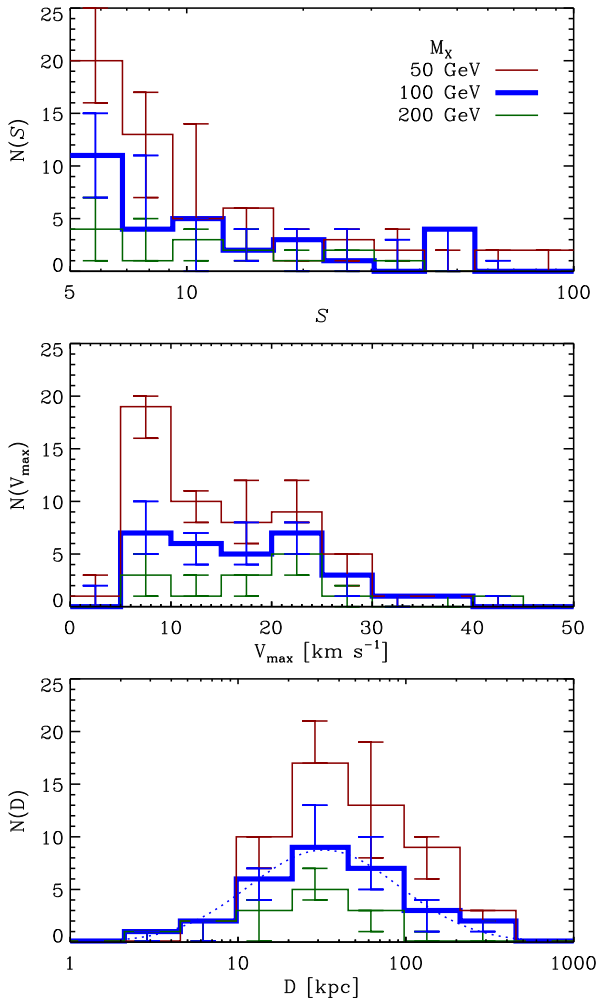


FIG. 10.— Differential distribution of detection significance $\mathcal{S}$ (*top*), $V_{\rm max}$ (*center*), and distance to the observer (*bottom*) of the subset of detectable ($\mathcal{S} > 5$) subhalos, for three different choices of M_χ (assuming $\langle\sigma v\rangle = 5 \times 10^{-26}$ cm^3 s^{-1}). The solid lines are for the fiducial observer placed along the intermediate axis of the host halo ellipsoid and the error bars indicate the range of values for 10 randomly chosen observer locations. For the distance distribution the best-fit Gaussian has been overplotted for the $M_\chi = 100$ GeV case.

For these, the median $V_{\rm max}$ is 24 km s^{-1}, indicating that the most detectable subhalos tend to be the more massive ones. These would be more likely to host a dwarf galaxy (e.g. Madau et al. 2008), which in some cases may have so far eluded discovery due to their ultra-faint optical surface brightness. The $V_{\rm max}$ distribution, however, reveals that a siginificant number of lower $V_{\rm max}$ subhalos should also be detectable. From 5 to 25 km s^{-1} the $V_{\rm max}$ distribution is approximately flat, and in the $M_\chi = 50$ GeV case it even exhibits a pronounced peak towards lower $V_{\rm max}$. No detectable subhalos are found with $V_{\rm max}$ less than 5 km s^{-1}, which is probably due to a lack of numerical resolution in these low mass halos. It appears likely that the total number of detectable subhalos has not yet converged in our simulations. We explore this further in Section 3.5 below.

The distance distribution of detectable subhalos is broadly peaked around the median of 40 kpc from the observer. For the $M_\chi = 100$ GeV case, it is consistent with a simple log-normal distribution, centered at 32 kpc with a width of $\sigma_{\log_{10} D} = 0.45$. About 80% of all detectable subhalos have distances between 10 and 100 kpc, and only 7.5% are closer than 10 kpc.

3.5. *Convergence?*

In Section 3.1 we discussed the diffuse background resulting from undetectable subhalos, but we should also consider whether any subhalos below VL-II's resolution limit of $10^6\,{\rm M}_\odot$ might be detectable as individual extended sources. The fact that the $V_{\rm max}$ distribution of detectable subhalos remains flat (or even rises slightly) down to the smallest visible subhalos hints that the number of detectable subhalos has not yet converged in our simulations. Further evidence comes from directly comparing the VL-II results with the lower resolution VL-I simulation. In VL-I we find far fewer detectable subhalos. In fact, with $\langle\sigma v\rangle = 3 \times 10^{-26}$ cm^3 s^{-1}, at most 15 subhalos are visible, and that only for the most optimistic assumptions. Typically only VL-I's most massive subhalo reaches $\mathcal{S} = 5$. The likely explanation for the dearth of detectable subhalos in VL-I is that the lower numerical resolution resulted in a significant suppression of substructure close to the center. In VL-I only 42 subhalos with at least 200 particles are closer than 50 kpc from the halo center, whereas in VL-II this number is 362, of which 108 are more massive than $4.2 \times 10^6\,{\rm M}_\odot$ (200 VL-I particles). Subhalos in VL-II also typically have higher central densities: the median of the maximum density in all subhalos with $M_{\rm sub} > 4.2 \times 10^6\,{\rm M}_\odot$ is 5.4 times higher in VL-II than in VL-I. This will lead to higher fluxes and hence increased detectability.

These considerations motivate a calculation of the total expected number of detectable subhalos below the simulation's resolution limit, including the full hierarchy of substructure all the way down to the free streaming cutoff m_0. Microhalos, the remnants of the earliest collapsed DM structures, are of particular interest here, as they have recently been suggested as possible GLAST sources that may even exhibit proper motion (Koushiappas 2006). In the following discussion we focus on resolved subhalos, because above the VL-II resolution the unresolved component is small, and, as we now show, the fraction of unresolved, detectable sources will further decrease with mass.

In the previous section we showed that in our simulations 95% of all detectable subhalos are extended sources covering more than one pixel. The fraction of point-like source is likely to become even smaller for less massive systems. For an NFW density profile, 87.5% of the annihilation luminosity is generated within the scale radius, hence r_s/D is a good proxy for a subhalo's angular size. Assuming an angular resolution of 9 arcmin, the maximum distance out to which a subhalo will appear extended is $D_{\rm max} = r_s/9$ arcmin $= 380\ r_s$. For a Bullock et al. (2001) concentration-mass relation $c(M) \propto M^{-0.025}$ for halos with masses below $10^6\,{\rm M}_\odot$. In this case

$$D_{\rm max} \propto r_s \propto R/c \propto M^{1/3} M^{0.025} \propto M^{0.358}. \qquad (15)$$

Specifically, assuming that local subhalos are three times

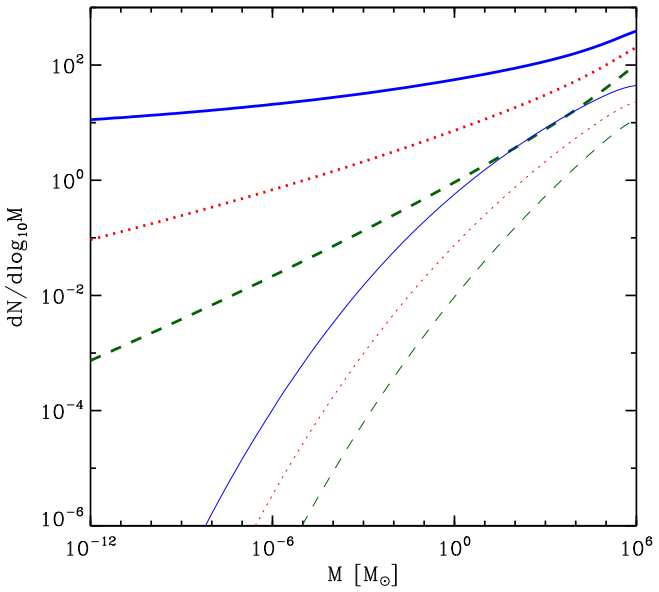


FIG. 11.— The differential mass function of extended (i.e. GLAST-resolvable, $r_s/D > 9$ arcmin, thick upper lines) and observable ($r_s/D > 9$ arcmin *and* $\Phi > 1$ GeV^2 kpc cm^{-6} sr^{-1}, thin lower lines) subhalos below VL-II's mass resolution of $10^6\,M_\odot$, for $\alpha = 2.0$ (solid), 1.9 (dotted), and 1.8 (dashed).

more concentrated than field halos (Eq. 14), we find

$$D_{\rm max} \approx 0.6 \left(\frac{M}{10^{-6}\,M_\odot}\right)^{0.358} {\rm pc}. \qquad (16)$$

At distances exceeding $D_{\rm max}$, sources appear point-like and the surface brightness in one pixel simply scales as L/D^2. For microhalos with $M < 1\,M_\odot$, $L \propto M^{0.93}$ and hence the maximum surface brightness of such unresolved sources scales with mass as $L/D^2_{\rm max} \propto M^{0.93} \times (M^{0.358})^{-2} \propto M^{0.214}$, resulting in a smaller fraction of detectable point-like sources for lower mass subhalos.

The differential mass function of extended (i.e. GLAST-resolvable) subhalos scales approximately as $dN_{\rm ext}/dM \propto dn_{\rm sub}/dM D^3_{\rm max} \sim M^{-\alpha+1.074}$, implying that even for $\alpha = 2.0$ the total number $N_{\rm ext}$ will be dominated by the most massive subhalos, i.e. those just below VL-II's resolution limit. The results of a more realistic calculation (details in Appendix B), taking into account the radial concentration bias and a log-normal concentration distribution at a given mass, are consistent with this simple scaling and are shown with the thick upper lines in Fig. 11. Integrating this differential extended source mass function from $m_0 = 10^{-6}\,M_\odot$ to $10^6\,M_\odot$, we find $N_{\rm ext} = 1090, 324, 115$ for α =2.0, 1.9, and 1.8, respectively.

Of course not all of these extended subhalos would actually be detectable by GLAST. We can extend the above calculation by imposing an additional constraint on the subhalo surface brightness. For an NFW density profile the surface brightness within r_s is given by

$$\Phi = \frac{L}{4\pi D^2 \pi (r_s/D)^2} = \frac{L}{4\pi^2 r_s^2} \approx \frac{0.875}{3\pi}\rho_s^2 r_s. \qquad (17)$$

Since $\rho_s \propto c^3/f(c)$, $\Phi \propto Rc^5/f(c)^2 \propto M^{1/3}c^5/f(c)^2$. Thus for a halo of a fixed mass, the surface brightness has a very steep concentration dependence, $\Phi \propto c^{4.316}$ for $M < 10^6\,M_\odot$. For this reason it is very important to account for the radial bias and the log-normal scatter in subhalo concentrations. A conservative choice for the limiting surface brightness for detection is $\Phi_0 = 1$ GeV^2 kpc cm^{-6} sr^{-1}, which is a bit below the minimum central brightness of all detectable subhalos in our study. The thin lower lines in Fig. 11 show how this additional constraint lowers the expected number of detectable extended microhalos. Lower mass halos are more strongly affected by a surface brightness cut, since Φ scales as $M^{0.225}$ for $c \propto M^{-0.025}$. In total we find the surface brightness constraint lowers the expected number of detectable subhalos with masses below $10^6\,M_\odot$ by about an order of magnitude to 82, 32, and 13 subhalos for α =2.0, 1.9, and 1.8, respectively. Thus we conclude that subhalos below VL-II's resolution limit contribute at most 3/4 of the expected total number of detectable extended sources.

Contrary to previous results (Koushiappas 2006), we find that GLAST is unlikely to be able to detect and resolve individual microhalos, defined here as subhalos with masses less than $1\,M_\odot$. According to our calculations, only 0.40, 0.042, and 0.0044 subhalos with masses between 10^{-6} and $1\,M_\odot$ would satisfy both angular size and surface brightness constraints. The disagreement between Koushiappas (2006) and our results is explained by our lower local subhalo abundance ($\xi = (M^2 dn/dM)/\rho_{\rm host}(R_\odot) = 8 \times 10^{-4}$ versus his 0.002), higher local concentrations resulting in smaller angular sizes, and a more realistic treatment of the expected backgrounds, including a contribution from undetectable subhalos. For comparison, we find that the local abundance of microhalos is (10.7, 0.388, 0.0137) pc^{-3} for $\alpha = (2.0, 1.9, 1.8)$ for the anti-biased radial subhalo distribution and (189, 6.83, 0.241) pc^{-3} in the unbiased case.

4. DISCUSSION AND CONCLUSION

In this work we have considered the possibility of directly observing Galactic DM substructure through the detection of gamma rays originating in the annihilation of DM particles in the centers of subhalos. Based on a hybrid approach, making use of both the highest resolution numerical simulations available as well as analytical models for the extrapolation beyond this simulation's resolution limit, we have shown that for reasonable values of the DM particle physics and subhalo mass function parameters, future gamma-ray observatories, such as the soon to be launched GLAST satellite, may very well be able to detect a few, even up to several dozen, such subhalos.

An important overall systematic uncertainty in our study is the nature of the DM particle. Our results are valid for the case of a weakly interacting relic particle, such as the lightest supersymmetric particle in supersymmetric extensions of the standard model. If the DM particle instead turns out to be an axion, for example, then DM annihilation would not occur and our results would be irrelevant. Even in the WIMP case, the allowed parameter space for the mass and annihilation cross section of the DM particle spans many orders of magnitude. Individual subhalos will only be detectable with GLAST, if M_χ and $\langle\sigma v\rangle$ fall in an "observable window", roughly

given by $M_\chi \sim 50 - 500$ GeV for $\langle\sigma v\rangle \sim 1 - 10 \times 10^{-26}$ cm^3 s^{-1}.

Another set of uncertainties is associated with our use of a numerical simulation. First of all, we have only simulated one host halo at very high resolution. Statistical studies at lower resolution (e.g. Reed et al. 2005) have found about a factor of two halo-to-halo scatter in the substructure abundance. Secondly, an uncertainty arises from the importance of DM substructure below the resolution limit of our simulation, due to its boosting effect on the brightness of individual subhalos, its contribution to a diffuse background from undetectable subhalos, and as individually detectable sources. Lastly, the lack of a baryonic component in our simulation is another source of uncertainty. In addition to the effects baryonic physics might have on the DM distribution at the Galactic center (see Section 2.3), one may worry that the abundance or detectability of nearby subhalos could be reduced by passages through the Milky Way's stellar disk. We can use the subhalo orbits from our simulations to constrain how large an effect such disk crossings would have.

For this estimate we have used orbits from the VL-I simulation (Diemand et al. 2007b; Kuhlen et al. 2007), as we are still in the process of extracting them from the VL-II dataset. We model the Milky Way's stellar disk as an exponential disk with scale radius $R_d = 3.5$ kpc and scale height $z_d = 350$ pc. Only 8.2% of all VL-I subhalos ever entered a central disk region delimited by four scale lengths, i.e. $R < 4R_d$ and $|z| < 4z_d$.[5] This fraction grows to 22% when only subhalos within 50 kpc of the halo center at $z = 0$ are considered. Only about one fifth of all disk crossing subhalos do so more than once. The median of V_z, the velocity component perpendicular to the disk, is quite large, about $400\,\mathrm{km\,s^{-1}}$. Since the typical disk crossing times are thus a few Myr, much less than the internal dynamical time of subhalos even within r_s (~ 100 Myr), we can apply the impulse approximation to determine how much subhalos will be heated by disk passages (see §7.2 of Binney & Tremaine 1987). The change in the z-component of the velocity of a DM particle belonging to a disk crossing subhalo is given by

$$\Delta V_z = \frac{2|z|}{V_z}|g_z(R)|, \tag{18}$$

where $|z|$ is the height of the particle above the subhalo's midplane and $g_z(R)$ is the gravitational field of the disk at radius R, and is approximately equal to $g_z(R) = 2\pi G\Sigma_0 \exp[(R_0 - R)/R_d]$. Here $\Sigma_0 \simeq 75\,\mathrm{M_\odot\,pc^{-2}}$ is the surface density of the disk in the solar neighborhood $R = R_0$. Setting $z = r_{\mathrm{Vmax}}$, we find

$$\Delta V_z(|z|) = 5\ \mathrm{km\,s^{-1}} \exp\left[\frac{R_0 - R}{R_d}\right] \times \left(\frac{|z|}{500\mathrm{pc}}\right)\left(\frac{V_z}{400\,\mathrm{km\,s^{-1}}}\right)^{-1}. \tag{19}$$

We can understand how destructive such kicks will be to the subhalo by comparing ΔV_z to the local circular velocity at height z. We find that for all disk crossings in VL-I the median of $(\Delta V_z/V_c)$ is 0.4 at $z = r_s$, and only 25% have $\Delta V_z > V_c$ at r_s. These numbers will be even smaller closer to the subhalo's center, since $\Delta V_z \propto z$ and $V_c \propto \sqrt{r}$. We conclude that only about 5% of all subhalos within 50 kpc today might have experienced a significant reduction in central density, and hence in annihilation luminosity, from disk crossings.

Given the substantial uncertainties discussed above, one may wonder whether it is even sensible to consider DM annihilations from subhalos at all. We believe that the mere possibility of detecting DM annihilations with GLAST offers such an exciting opportunity to directly confirm the existence of a DM particle and to learn something about its properties, that it warrants theoretical investigations such as the present one.

We conclude by summarizing our main findings:

- Numerical simulations indicate that DM is far from smoothly distributed throughout the Galactic halo. Extremely high resolution simulations, such as the Via Lactea series, have shown that this clumpiness extends into individual subhalos, resulting in sub-substructure. Since the annihilation rate is proportional to the DM density squared, such clumpiness leads to a boost by $(1 + B(M))$ of the annihilation luminosity compared to a smooth density distribution. Any determination of the gamma-ray brightness of individual subhalos must account for this boost factor. In the case of simulated subhalos only the portion of the sub-substructure hierarchy below the simulation's resolution limit should be included in the boost factor calculation. Our analytical model of the boost factor, which assumes a powerlaw subhalo mass function of slope α and low-mass cutoff m_0, a resolved subhalo mass fraction of 10%, and a Bullock et al. (2001) like concentration-mass relation, results in moderate boost factors of a few up to 10 for $(\alpha, m_0) = (2.0, 10^{-6})$. Lowering m_0 to 10^{-12} raises $B(M)$ by a factor of 2. For $\alpha = 1.9$ $B(M)$ barely exceeds unity.

- The portion of the substructure hierarchy below Via Lactea's resolution also contributes to a diffuse annihilation background from undetectable sources. The magnitude of this background depends on the spatial distribution of subhalos within the host halo in addition to the subhalo mass function parameters (α, m_0). We have extended the model developed by Pieri et al. (2008) to allow for an anti-biased subhalo radial distribution and for higher subhalo concentrations closer to the host halo center. The resulting background tends to dominate the diffuse background from the smooth host halo at angles greater than $\psi = 10^\circ - 60^\circ$, depending on the choice of (α, m_0). At high galactic latitudes this background can dominate the astrophysical backgrounds (both Galactic and extragalactic) and should be accounted for when determining subhalo detectability.

- By comparing the expected number of gamma-ray photons from an individual subhalo to the square root of the number of expected background photons, we can determine a detection significance $\mathcal{S}$ for each subhalo. $\mathcal{S}$ depends strongly on the

[5] For simplicity we aligned the disk with the z-axis, but the results are insensitive to this choice.

mass M_χ and annihilation cross section $\langle\sigma v\rangle$ of the DM particle as well as on the subhalo mass function parameters (α, m_0). We find that for $M_\chi \sim 50 - 500$ GeV and $\langle\sigma v\rangle \sim 1 - 10 \times 10^{-26}$ cm^3 s^{-1}, a few subhalos, even up to a few tens, exceed $\mathcal{S} = 5$, and hence should be detectable with GLAST. In the most optimistic case we considered ($M_\chi = 100$ GeV, $\langle\sigma v\rangle = 10^{-25}$ cm^3 s^{-1}, $\alpha = 2.0$, and $m_0 = 10^{-12}\,\mathrm{M}_\odot$) almost 100 subhalos would be detectable, whereas increasing M_χ to 500 GeV or lowering $\langle\sigma v\rangle$ to 10^{-26} cm^3 s^{-1} sharply reduces the expected number of sources, especially for low α or high m_0.

- For the particular DM annihilation model that Hooper et al. (2007) proposed to explain the WMAP haze, an excess microwave emission around the Galactic center, namely $M_\chi \sim 100$ GeV, $\langle\sigma v\rangle = 3 \times 10^{-26}$ cm^3 s^{-1}, and a central host halo density cusp of slope -1.2, we find that GLAST should be able to detect around 15 subhalos, for reasonable choices of (α, m_0).

- Th majority of all detectable subhalos are resolved with GLAST's expected angular resolution of 9 arcmin. The median number of pixels is 13, and only 5% are detected in only one pixel.

- For 9 out of the 11 observer locations we considered, the angular distribution of detectable subhalos is consistent with an isotropic distribution on the sky.

- Those subhalos that are detected with the highest significances ($\mathcal{S} > 25$) tend to be the more massive ones, with a median $V_{\max}$ of 24 km s^{-1}. However, the $V_{\max}$ distribution of detectable subhalos is flat, or slightly rising, towards lower $V_{\max}$, down to $V_{\max} = 5$ km s^{-1}.

- Detectable subhalos typically lie between 10 and 100 kpc from the observer. The distance distribution is consistent with a log-normal distribution centered at 32 kpc and a width of $\sigma_{\log_{10} D} = 0.45$.

- It appears that the number of detectable subhalos has not yet converged in our simulations. Higher resolution simulations would likely resolve smaller clumps, which are more abundant and more likely to be found near the observer. We estimate that we may be missing up to three quarters of all detectable subhalos.

Our results suggest that searching for Galactic DM substructure should be an important part of the GLAST data analysis in the upcoming years.

We would like to thank our collaborators Ben Moore, Doug Potter, Joachim Stadel, and Marcel Zemp for their help and assistance with code development and testing, and for allowing the use of the Via Lactea II dataset prior to publication. This work benefited from fruitful discussions with Bill Atwood, Sergio Colafrancesco, Miguel Sánchez-Conde, Dan Hooper, Robert Johnson, Savvas Koushiappas, Stefano Profumo, Louie Strigari, Andrew Strong, and Scott Tremaine. Support for this work was provided by NASA grants NAG5-11513 and NNG04GK85G. M.K. gratefully acknowledges support from the Hansmann Fellowship at the Institute for Advanced Study. J.D. acknowledges support from NASA through Hubble Fellowship grant HST-HF-01194.01. The "Via Lactea I" simulation was performed on NASA's *Project Columbia* supercomputer. "Via Lactea II" was performed on the *Jaguar* Cray XT3 supercomputer at the Oak Ridge National Laboratory, through an award from DOE's Office of Science as part of the 2007 Innovative and Novel Computational Impact on Theory and Experiment (INCITE) program. It is a pleasure to thank Bronson Messner and the Scientific Computing Group at the National Center for Computational Sciences for their help and assistance.

REFERENCES

Aharonian, F., et al. 2006, Physical Review Letters, 97, 221102
Albert, J., et al. 2006, ApJ, 638, L101
Albert, J., et al. 2008, ApJ, 679, 428
Aloisio, R., Blasi, P., & Olinto, A. V. 2004, ApJ, 601, 47
Athanassoula, E., Ling, F. -., Nezri, E., & Teyssier, R. 2008, ArXiv e-prints, 801, arXiv:0801.4673
Baltz, E. A., Briot, C., Salati, P., Taillet, R., & Silk, J. 2000, Phys. Rev. D, 61, 02351
Baltz, E. A., & Wai, L. 2004, Phys. Rev. D, 70, 023512
Baltz, E. A., Taylor, J. E., & Wai, L. L. 2007, ApJ, 659, L1254
Berezinsky, V., Bottino, A., & Mignola, G. 1994, Physics Letters B, 325, 136
Bergström, L., & Ullio, P. 1997, Nuclear Physics B, 504, 27
Bergström, L., Ullio, P., & Buckley, J. H. 1998, Astroparticle Physics, 9, 137
Bergström, L., Edsjö, J., Gondolo, P., & Ullio, P. 1999, Phys. Rev. D, 59, 043506
Bergström, L., Edsjö, J., & Ullio, P. 2001, Physical Review Letters, 87, 251301
Bertone, G., Hooper, D., & Silk, J. 2005, Phys. Rep., 405, 279
Bertone, G., Zentner, A. R., & Silk, J. 2005, Phys. Rev. D, 72, 103517
Binney, J., & Tremaine, S. 1987, Princeton, NJ, Princeton University Press, 1987
Blumenthal, G. R., Faber, S. M., Flores, R., & Primack, J. R. 1986, ApJ, 301, 27
Bringmann, T., Bergström, L., & Edsjö, J. 2008, Journal of High Energy Physics, 1, 49
Bullock, J. S., et al. 2001, MNRAS, 321, 559
Calcáneo-Roldán, C., & Moore, B. 2000, Phys. Rev. D, 62, 123005
Cesarini, A., Fucito, F., Lionetto, A., Morselli, A., & Ullio, P. 2004, Astroparticle Physics, 21, 267
Chiang, J., & Mukherjee, R. 1998, ApJ, 496, 752
Colafrancesco, S., Profumo, S., & Ullio, P. 2006, A&A, 455, 21
Colafrancesco, S., Profumo, S., & Ullio, P. 2007, Phys. Rev. D, 75, 023513
Dermer, C. D. 2007, ApJ, 659, 958
Diemand, J., Moore, B., & Stadel, J. 2004, MNRAS, 353, 624
Diemand, J., Moore, B., Stadel, J., & Kazantzidis, S. 2004, MNRAS, 348, 977
Diemand, J., Zemp, M., Moore, B., Stadel, J., & Carollo, C. M. 2005, MNRAS, 364, 665
Diemand, J., Madau, P., & Moore, B. 2005, MNRAS, 364, 367
Diemand, J., Kuhlen, M., & Madau, P. 2006, ApJ, 649, 1
Diemand, J., Kuhlen, M., & Madau, P. 2007, ApJ, 657, 262
Diemand, J., Kuhlen, M., & Madau, P. 2007, ApJ, 667, 859
Diemand, J., Kuhlen, M., Madau, P., Zemp, M., Moore, B., Potter, D., Stadel, J. 2008, Nature, in press

Driscoll, D. D., et al. (STACEE Collaboration) 2007, ArXiv e-prints, 710, arXiv:0710.3545
Dutton, A. A., van den Bosch, F. C., Dekel, A., & Courteau, S. 2007, ApJ, 654, 27
Evans, N. W., Ferrer, F., & Sarkar, S. 2004, Phys. Rev. D, 69, 123501
Finkbeiner, D. P. 2004, ApJ, 614, 186
Fornengo, N., Pieri, L., & Scopel, S. 2004, Phys. Rev. D, 70, 103529
Giommi, P., Colafrancesco, S., Cavazzuti, E., Perri, M., & Pittori, C. 2006, A&A, 445, 843
Gnedin, O. Y., Kravtsov, A. V., Klypin, A. A., & Nagai, D. 2004, ApJ, 616, 16
Gnedin, O. Y., & Primack, J. R. 2004, Physical Review Letters, 93, 061302
Gondolo, P., Edsjö, J., Ullio, P., Bergström, L., Schelke, M., & Baltz, E. A. 2004, Journal of Cosmology and Astro-Particle Physics, 7, 8]
Green, A. M., Hofmann, S., & Schwarz, D. J. 2005, JCAP, 8, 3
Hartman, R. C., et al. 1999, ApJS, 123, 79
Hooper, D., & Dingus, B. L. 2004, Phys. Rev. D, 70, 113007
Hooper, D., Finkbeiner, D. P., & Dobler, G. 2007, Phys. Rev. D, 76, 083012
Hunter, S. D., et al. 1997, ApJ, 481, 205
Jungman, G., Kamionkowski, M., & Griest, K. 1996, Phys. Rep., 267, 195
Klypin, A., Kravtsov, A. V., Valenzuela, O., & Prada, F. 1999, ApJ, 522, 82
Koushiappas, S. M., Zentner, A. R., & Walker, T. P. 2004, Phys. Rev. D, 69, 043501
Koushiappas, S. M. 2006, Physical Review Letters, 97, 191301
Kuhlen, M., Strigari, L. E., Zentner, A. R., Bullock, J. S., & Primack, J. R. 2005, MNRAS, 357, 387
Kuhlen, M., Diemand, J., & Madau, P. 2007, ApJ, 671, 1135
Lavalle, J., Yuan, Q., Maurin, D., & Bi, X.-J. 2008, A&A, 479, 427
Loeb, A., & Zaldarriaga, M. 2005, PRD, 71, 103520
Macciò, A. V., Dutton, A. A., van den Bosch, F. C., Moore, B., Potter, D., & Stadel, J. 2007, MNRAS, 378, 55
Madau, P., Diemand, J., & Kuhlen, M., 2008, ApJ, in press
Merritt, D., Milosavljević, M., Verde, L., & Jimenez, R. 2002, Physical Review Letters, 88, 191301
Moore, B., Ghigna, S., Governato, F., Lake, G., Quinn, T., Stadel, J., & Tozzi, P. 1999, ApJ, 524, L19
Moskalenko, I. V., Strong, A. W., Ormes, J. F., & Potgieter, M. S. 2002, ApJ, 565, 280
Pieri, L., Bertone, G., & Branchini, E. 2008, MNRAS, 384, 1627
Profumo, S. 2005, Phys. Rev. D, 72, 103521
Profumo, S., Sigurdson, K., & Kamionkowski, M. 2006, Physical Review Letters, 97, 031301
Reed, D., Governato, F., Quinn, T., Gardner, J., Stadel, J., & Lake, G. 2005, MNRAS, 359, 153
Sánchez-Conde, M. A., Prada, F., Łokas, E. L., Gómez, M. E., Wojtak, R., & Moles, M. 2007, Phys. Rev. D, 76, 123509
Sjöstrand, T., Edén, P., Friberg, C., Lönnblad, L., Miu, G., Mrenna, S., & Norrbin, E. 2001, Computer Physics Communications, 135, 238
Spergel, D. N., et al. 2007, ApJS, 170, 377
Sreekumar, P., et al. 1998, ApJ, 494, 523
Stecker, F. W., & Salamon, M. H. 1996, ApJ, 464, 600
Stoehr, F., White, S. D. M., Springel, V., Tormen, G., & Yoshida, N. 2003, MNRAS, 345, 1313
Strigari, L. E., Koushiappas, S. M., Bullock, J. S., & Kaplinghat, M. 2007, PRD, 75, 083526
Strigari, L. E., Koushiappas, S. M., Bullock, J. S., Kaplinghat, M., Simon, J. D., Geha, M., & Willman, B. 2007, ArXiv e-prints, 709, arXiv:0709.1510
Strong, A. W., & Moskalenko, I. V. 1998, ApJ, 509, 212
Strong, A. W., Moskalenko, I. V., & Reimer, O. 2004, ApJ, 613, 962
Strong, A. W., Moskalenko, I. V., Reimer, O., Digel, S., & Diehl, R. 2004, A&A, 422, L47
Tasitsiomi, A., & Olinto, A. V. 2002, Phys. Rev. D, 66, 083006
Taylor, J. E., & Silk, J. 2003, MNRAS, 339, 505
Ullio, P., Bergström, L., Edsjö, J., & Lacey, C. 2002, Phys. Rev. D, 66, 123502
Wechsler, R. H., Bullock, J. S., Primack, J. R., Kravtsov, A. V., & Dekel, A. 2002, ApJ, 568, 52
Weinberg, M. D., & Katz, N. 2007, MNRAS, 375, 460
Zemp, M., Stadel, J., Moore, B., & Carollo, C. M. 2007, MNRAS, 376, 273
Zentner, A. R., & Bullock, J. S. 2003, ApJ, 598, 49

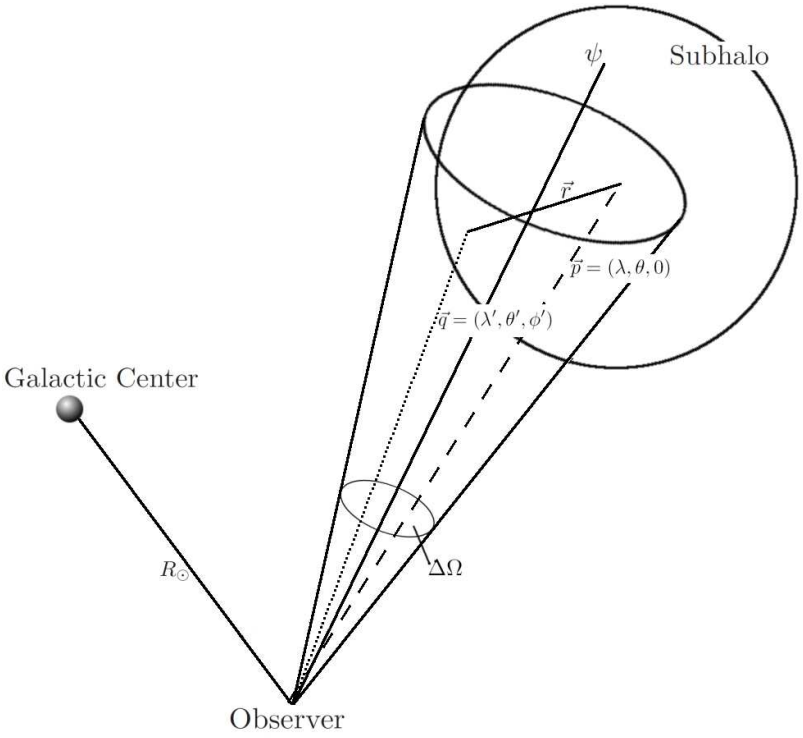


FIG. 12.— Diagram of the relevant geometry for the calculation of $\mathcal{F}_{\rm halo}$ (Eq. A8).

APPENDIX

A. CALCULATION OF THE DIFFUSE FLUX FROM INDIVIDUALLY UNDETECTABLE SUBHALOS

We follow the methodology presented in Pieri et al. (2008), and define the diffuse flux from individually undetectable subhalos from a solid angle $\Delta\Omega$ around the direction of observation ψ by

$$\mathcal{F}(\psi, \Delta\Omega) = \int_{\Delta\Omega} d\cos\theta \, d\phi \int_M dM \int_{\rm l.o.s.} d\lambda \, \lambda^2 \int_c dc \, P(c; M, R) \, \mathcal{F}_{\rm halo}(M, c, \lambda, \Delta\Omega) \, \frac{dn_{\rm sub}}{dM}(M, R), \tag{A1}$$

where λ is the distance along the line of sight and $R(\psi, \lambda, \theta, \phi)$ is the Galacto-centric distance, given by

$$R(\psi, \lambda, \theta, \phi) = \sqrt{\lambda^2 + R_\odot^2 - 2\lambda R_\odot(\cos\theta\cos\psi - \cos\phi\sin\theta\sin\psi)}. \tag{A2}$$

The subhalo mass function and spatial distribtution is given by

$$\frac{dn_{\rm sub}}{dM}(M, R) = AM^{-\alpha} \frac{1}{(1 + R/r_s^{\rm MW})^2} \, {\rm M}_\odot^{-1} \, {\rm kpc}^{-3}, \tag{A3}$$

and we have normalized it such that the total mass in subhalos with masses between $m_0 = 10^{-5} M_{\rm halo}$ and $m_1 = 10^{-2} M_{\rm halo}$ is 10% of $M_{\rm halo}$, i.e.

$$\int_{m_0}^{m_1} dM M \int_0^{r_{200}} 4\pi R^2 \frac{dn_{\rm sub}}{dM}(M, R) \, dR = 0.1 M_{\rm halo}. \tag{A4}$$

Note that this anti-biased spatial distribution is motivated by numerical simulations (Kuhlen et al. 2007; Madau et al. 2008) and differs from the distribution chosen by Pieri et al. (2008), who employed an unbiased distribution of the form

$$\frac{dn_{\rm sub}}{dM}(M, R) = AM^{-2} \frac{\mathcal{H}(R - r_{\rm min}(M))}{(R/r_s^{\rm MW})(1 + R/r_s^{\rm MW})^2} \, {\rm M}_\odot^{-1} \, {\rm kpc}^{-3}, \tag{A5}$$

where a Heaviside function $\mathcal{H}(R - r_{\rm min}(M))$ accounts for the tidal destruction of subhalos below a radius $r_{\rm min}(M)$. The subhalo concentration-mass relation $P(c; M, R)$ is based on the Bullock et al. (2001) model ($F = 0.01$ and $K = 3.75$) to which we have added a radial dependence of the form

$$c_0^{\rm sub}(M, R) = c_0^{\rm B01}(M) \left(\frac{R}{r_{200}} \right)^{-0.286}, \tag{A6}$$

which we have determined directly from our numerical simulations (Diemand et al. 2005b, 2008). With this scaling, subhalos at $R_\odot$ are three times as concentrated as field halos. Note that we include a log-normal scatter of width $\sigma_{\log_{10} c} = 0.14$, such that

$$P(c; M, R) = \frac{1}{c \ln 10} \frac{1}{\sqrt{2\pi}\sigma_{\log_{10} c}} \exp\left[-\frac{(\log_{10} c - \log_{10} c_0^{\rm sub})^2}{2\,\sigma^2_{\log_{10} c}}\right]. \tag{A7}$$

The flux in a solid angle $\Delta\Omega$ around ψ originating from a subhalo of mass M at a position (λ, θ, ϕ) is given by

$$\mathcal{F}_{\rm halo}(M, c, \lambda, \theta, \phi, \Delta\Omega) = \int_{\Delta\Omega} d\cos\theta'\, d\phi' \int_{\rm l.o.s.} \lambda'^2\, \frac{\rho^2(M, c, r(\lambda, \theta, \phi, \lambda', \theta', \phi'))}{4\pi\lambda'^2}\, d\lambda', \tag{A8}$$

where the subhalo's density profile is given by an NFW profile with a constant core below $r_c = 10^{-8}$ kpc:

$$\rho(M, c, r) = \begin{cases} \frac{\rho_s}{(r/r_s)(1+r/r_s)^2} & \text{for } r > r_c \\ \frac{\rho_s}{(r_c/r_s)(1+r_c/r_s)^2} & \text{for } r \le r_c. \end{cases} \tag{A9}$$

The NFW scale density ρ_s depends only on c, and the scale radius r_s on M and c. We have checked that our results are not strongly dependent on the value of r_c: $\mathcal{F}$ changes by less than 1% for r_c between 10^{-9} kpc and 10^{-7} kpc.

Fig.12 shows a diagram of the geometry relevant for the calculation of $\mathcal{F}_{\rm halo}$. Without loss of generality we can choose a coordinate system in which $\phi = 0$ for the position $\vec{p}$ of a given subhalo, and hence $\mathcal{F}_{\rm halo}$ is independent of ϕ. The distance r from the center of the subhalo at $\vec{p} = (\lambda, \theta, 0)$ to the point $\vec{q} = (\lambda', \theta', \phi')$ within the cone of integration is

$$r(\lambda, \theta, \lambda', \theta', \phi') = \sqrt{\lambda^2 + \lambda'^2 - 2\lambda\lambda'\,(\sin\theta \sin\theta' \cos\phi' + \cos\theta\cos\theta')}. \tag{A10}$$

We are integrating over a very small opening angle $\Delta\Omega = 4.36 \times 10^{-6}$ sr, corresponding to $\theta_{\rm max} = 1.2 \times 10^{-3}$, and hence we are justified in setting $\sin\theta = 0$ and $\cos\theta = 1$, i.e. placing the subhalo on the line of sight given by ψ. In this case $\mathcal{F}_{\rm halo}$ depends only on M, c, λ, and $\Delta\Omega$, and is given by

$$\mathcal{F}_{\rm halo}(M, c, \lambda, \Delta\Omega) = \frac{\rho_s^2 r_s}{2} \int_{\cos\theta_{\rm max}}^1 d\cos\theta' \int_0^\infty \frac{1}{(\xi^2 + \xi'^2 - 2\xi\xi'\cos\theta')\left(1 + \sqrt{\xi^2 + \xi'^2 - 2\xi\xi'\cos\theta'}\right)^4}\, d\xi', \tag{A11}$$

where $\xi = \lambda/r_s$ and $\xi' = \lambda'/r_s$.

B. CALCULATION OF DETECTABLE AND EXTENDED SUBHALO MASS FUNCTIONS

The mass function of extended subhalos is given by

$$\frac{dN_{\rm res}}{dM} = \int_{4\pi} d\cos\theta\, d\phi \int d\lambda\, \lambda^2 \int dc\, P(c; M, R)\, \frac{dn_{\rm sub}}{dM}(M, R)\, \mathcal{H}(D_{\rm max}(M, c) - \lambda), \tag{B1}$$

where λ, R, $P(c; M, r)$, and $dn_{\rm sub}/dM$ are defined as in Eq. A1 (with $\psi = 0$), $\mathcal{H}$ is the Heaviside step function, and

$$D_{\rm max} = r_s/9 \text{ arcmin} = 10 \text{ kpc} \frac{1}{c(M, R)} \left(\frac{M}{1\,{\rm M}_\odot}\right)^{1/3} \tag{B2}$$

is the maximum distance out to which a subhalo of mass M and concentration $c(M, R)$ would appear extended. An additional constraint on the surface brightness Φ can be incorporated by introducing a second Heaviside step function, $\mathcal{H}(\Phi - \Phi_0)$.